Automotive Experiences
Vol. 8 No. 1 (2025) pp. 122-145
p-ISSN: 2615-6202 e-ISSN: 2615-6636

Research Paper

Vehicle Trajectory Analysis on the Effect of Additional Load Distribution Disturbance at Different Speeds for Collision Avoidance Systems

Abdullah bin Zulkifli[1], **Mohamad Heerwan bin Peeie**[1,2], **Muhammad Izhar bin Ishak**[1,2]

[1]Faculty of Mechanical & Automotive Engineering Technology, Universiti Malaysia Pahang Al-Sultan Abdullah, 26600 Pekan, Pahang, Malaysia
[2]Centre for Automotive Engineering, Universiti Malaysia Pahang Al-Sultan Abdullah, 26600 Pekan, Pahang, Malaysia

mheerwan@umpsa.edu.my

https://doi.org/10.31603/ae.13200

Published by Automotive Laboratory of Universitas Muhammadiyah Magelang

Article Info
Submitted: 19/02/2025
Revised: 10/03/2025
Accepted: 26/03/2025
Online first: 13/04/2025

Abstract

Collision avoidance (CA) systems have become a requirement in vehicles due to their ability to prevent collisions. Despite the implementation of these systems on the road, accidents still happen due to the lack of adaptability of CA systems corresponding to road environment nonlinearities and external disturbances. Hence, this research focuses on the effect of external disturbances, such as additional load distribution on the vehicle while avoiding obstacles. The deployment of the CA scenario, considering the presence of disturbance, was simulated in MATLAB Simulink, with the reference trajectory for the system obtained from a skilled driver in real-time experiments at different speeds. The objective of this study is to observe and analyse the effect of additional load disturbances on vehicle stability, especially when the driver countersteers to avoid an obstacle. An increase in the additional load percentage at each side of the vehicle produces excessive lateral force opposite to the direction of the vehicle. This scenario creates a significant load transfer phenomenon and directly causes the vehicle to oversteer and understeer while avoiding obstacles. It has been observed that human cognition plays a huge role in defining a reference trajectory at different speeds while avoiding an obstacle. The pattern of the reference trajectory also affects the magnitude of the load transfer phenomena, especially when the driver manoeuvres the vehicle aggressively.

Keywords: Collision avoidance; Additional load distribution disturbance; Vehicle stability; Human cognitive driving behaviour

1. Introduction

In Malaysia and many other developing nations, traffic accidents are among the leading causes of death [1], [2], [3], [4]. The World Health Organization (WHO) ranks road traffic accidents as the ninth most prevalent cause of fatalities worldwide [5], [6]. Furthermore, throughout Malaysia's Movement Control Order (MCO) operation period, which ran from March 18, 2020, to October 13, 2021, 566,760 accidents have been documented, of which 5,412 were fatal, resulting in 5,739 fatalities, according to Federal Traffic Investigation and Enforcement Department director Datuk Mat Kasim Karim [7]. According to WHO estimates, road traffic accidents may claim the lives of 1.3 million people each year, and the trend indicates that the number of road traffic accident fatalities in Malaysia is rising [1]. The causes of road traffic accidents can be grouped into three main categories: human error, environmental factors, and vehicle features [8].

One main component contributing to road traffic accidents is human error. A study revealed that human error accounts for 90% of road traffic accidents [9]. Road traffic accidents are primarily caused by human mistakes related to poor driving

This work is licensed under a Creative Commons Attribution-NonCommercial 4.0 International License.

habits, inexperience, drug use, and overloading [10], [11]. Numerous research studies have been carried out, and various mitigation mechanisms, such as cruise control and lane-keeping assistance, have been implemented to reduce the negative effects of negligent driving practices [12]. Prior to 2015, notably in the United States, 80–94% of collisions were attributed to irresponsible driving, while 33% resulted from other drivers' inaccurate estimations [13]. The examination of traffic accidents and their underlying causes leads us back to human drivers, whose behaviours are diverse and complex. According to [11], [14], using humans as solutions in crisis situations may involve using them as social agents, road users, transport customers, and psychobiological organisms. In addition to skills relevant to vehicle handling, a human driver may also possess specific cognitive traits like attention, perceptual strength, responsiveness, judgement ability, and training-based capabilities. Alcohol-related driving behaviours may have also contributed to the occurrence of crashes [11], [15].

Weather, road geometry, uneven road conditions, and slick road surfaces are examples of environmental conditions. A study was carried out to determine how road conditions affect rollover incidents [16]. Rollovers and skidding are two types of traffic accidents that are caused by weather and road conditions. On slippery surfaces, a car skids quickly as there is less contact between the tyres and the road [16]. In contrast, vehicle features are mostly concerned with mechanical aspects, such as the engine, powertrain, brakes, and gross vehicle weight. The effect of gross vehicle weight on vehicle stability during cornering was investigated in [8]. The findings suggest that an increase in gross vehicle weight contributes to lateral instability in larger vehicles.

Autonomous collision avoidance (CA) is a mechanism designed to assist drivers in preventing collisions. Among the most complex systems within the Advanced Driver Assistance Systems is CA technology. The National Highway Traffic Safety Board recognised this technology as a safe system in 2016 [12], [17]. Despite significant advancements in the field of CA, several shortcomings remain that necessitate further development and enhancement. An area of concern is the effectiveness of CA implementations in real-world scenarios [18]. Given that traffic accidents can occur under a variety of circumstances, a good CA system should be able to direct the host vehicle's avoidance navigation across multi-scenario risks [18], [19], [20]. For instance, collision mitigation of a priori unknown barriers, high-speed highway crashes, intersection collisions, and CA in densely populated metropolitan areas [21], [22].

The development of a CA system must consider vehicle stability. For many years, stability has been a primary concern in vehicle design [8]. Automobiles are often susceptible to unknowns that can lead to instability and collisions [20]. The instability problems with electric vehicles and traditional internal combustion engine vehicles are comparable. A comprehensive understanding of the different types of stability and the state of vehicle stability is essential. Active driver assistance systems are becoming increasingly prevalent as they reduce the likelihood of collisions [21]. Anti-lock braking systems, electronic stability control, adaptive cruise control, active rollover protection, and forward collision warning systems are several examples of such active systems. Analysing vehicle stability requires consideration of three types of motion: lateral, longitudinal, and vertical.

The impact of varying vehicle loads (number of passengers) on the efficiency of the proposed integrated nonlinear CA control system was examined [23]. The fluctuations in host vehicle loads were used to assess the robustness of the controller design: the vehicle's basic kerb weight (the weight of the vehicle plus the driver); five-seated passengers, which add 20% to the vehicle weight, and fully-seated passengers with luggage, which add the vehicle load by 36% [23]. The researchers in [24] conducted a study by applying an additional load to the left side of the wheel while making a right turn. The study indicates that the increased longitudinal and lateral tyre forces result from the higher load placed on the vehicle's side during lateral motion. The findings suggest that the vehicle may crash when the load on the right side of the vehicle exceeds a specific threshold. A constant increase in longitudinal force generated at the tyres indicates that the tyre slip ratio exceeds one. For stable driving conditions, the tyre slip ratio must not exceed one. Thus, it can be inferred that the longitudinal and lateral forces of the tyres may increase when the load is elevated on the same side of the vehicle during lateral motion [24]. When the load surpasses a certain point, the vehicle becomes unstable.

An emergency lane change while avoiding an obstacle requires careful consideration of the vehicle's lateral stability. The phase-plane method, a classical technique for determining the stability of control systems, is frequently employed to estimate a vehicle's lateral stability during driving [20]. Reducing the vehicle's yaw and sideslip is crucial to preventing it from veering off track and colliding with obstacles. Researchers have developed several techniques to estimate vehicle sideslip angles, including integration, model estimation, neural network algorithms, fuzzy logic, and global positioning system (GPS)-based estimates [25]. Lyapunov's secondary approach, which is based on a two degrees-of-freedom dynamics model, was used in [26] to identify the lateral stability region of vehicles. In recent years, the research literature on CA extensively employed this stabilisation prediction approach, as stated in [27]. Researchers in [28] defined the stability region as the steering angle limit derived from the lateral properties of the tyres. All of these stabilisation evaluation methods have the limitation of the vehicle's sideslip angle to a minimal value. Consequently, these techniques sacrifice some agility in favour of a more cautious stability zone [20].

This study presents the results of a simulation aimed at analysing the dynamic behaviour and stability of a vehicle during the presence of additional load for CA on dry pavement at different speeds. The conclusions drawn from this study provide valuable guidance to manufacturers and researchers involved in the development of autonomous CA systems, particularly in the field of vehicle stability and control systems. This paper consists of a detailed analysis of the vehicle model description, followed by specifications of the experimental vehicle and the CA condition. Subsequently, the vehicle's trajectory was analysed in relation to human cognitive driving behaviour at different speeds, following the validation of the model. Finally, the effect of additional load disturbances on the vehicle's trajectory while avoiding an obstacle was analysed with respect to stability characteristics.

2. Analysis of Vehicle Model

2.1. Nonlinear Dynamic Vehicle Model

A nonlinear vehicle model combines the lateral and longitudinal forces acting on the vehicle. However, several factors must be considered when modelling these combined forces. **Figure 1** illustrates how the front tyre orients from its initial axis due to input from the steer wheel angle, δ, which consequently changes the orientation of the force axis. Eq. (1) to Eq. (3) represent the longitudinal, lateral, and yaw motions derived from **Figure 1**, respectively. The variables m, $\ddot{x}$, $\ddot{y}$, $\dot{x}$, $\dot{y}$, and $\dot{\varphi}$ represent the mass of the vehicle, the vehicle's longitudinal acceleration, the vehicle's lateral acceleration, the vehicle's longitudinal velocity, the vehicle's lateral velocity, and the vehicle's yaw rate, respectively. The variables F_{xfl}, F_{xfr}, F_{xrl}, and F_{xrr} represent the longitudinal force at the front left, front right, rear left, and rear right tyres, respectively, whereas F_{yfl}, F_{yfr}, F_{yrl}, and F_{yrr} represent the lateral force at the front left, front right, rear left, and rear right tyres, respectively. Accordingly, l_f and l_r represent the longitudinal distances between the C.G. and the front and rear tyres, respectively, whereas d_w denotes the track width.

2.2. Nonlinear Tyre Characteristics

The primary forces acting on the car are generated by the forces and moments from the road acting on each tyre. As car tyres are not stiff, the vertical stress on them causes them to deform quickly [29]. Three variables must be established before the forces can be calculated using Dugoff's tyre model. The initial parameter is the tyre slip

$$m\ddot{x} = \left(F_{xfl} + F_{xfr}\right)\cos\delta + F_{xrl} + F_{xrr} - \left(F_{yfl} + F_{yfr}\right)\sin\delta + m\dot{\varphi}\dot{y} \tag{1}$$

$$m\ddot{y} = F_{yrl} + F_{yrr} + \left(F_{xfl} + F_{xfr}\right)\sin\delta + \left(F_{yfl} + F_{yfr}\right)\cos\delta - m\dot{\varphi}\dot{x} \tag{2}$$

$$\begin{aligned} I_z\ddot{\varphi} = {} & l_f\left(F_{xfl} + F_{xfr}\right)\sin\delta + l_f\left(F_{yfl} + F_{yfr}\right)\cos\delta - l_r\left(F_{yrl} + F_{yrr}\right) + \frac{d_w}{2}\left(F_{xfr} - F_{xfl}\right)\cos\delta \\ & + \frac{d_w}{2}\left(F_{xrr} - F_{xrl}\right) + \frac{d_w}{2}\left(F_{yfl} - F_{yfr}\right)\sin\delta \end{aligned} \tag{3}$$

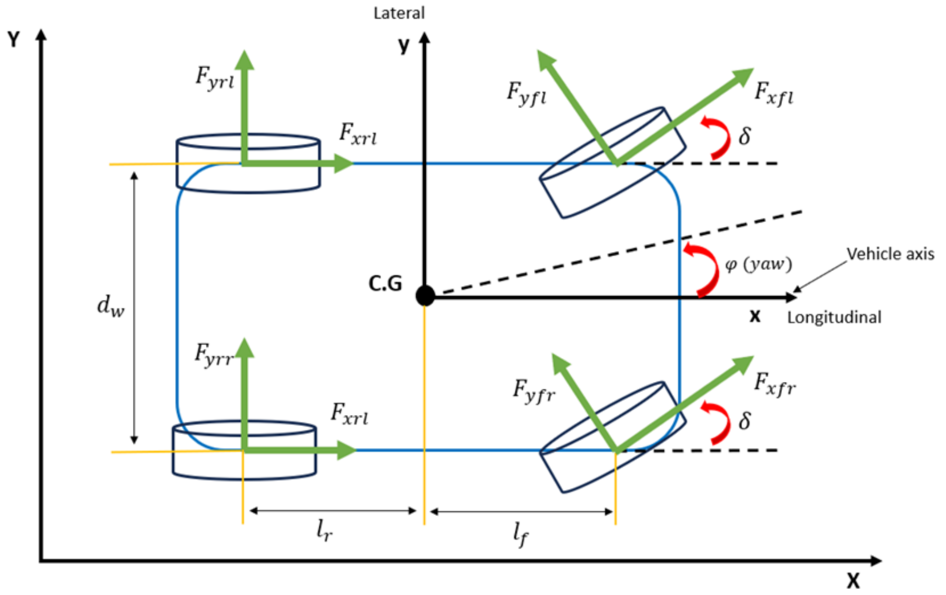

Figure 1. Force vector of nonlinear vehicle model

ratio, which refers to the difference between the longitudinal velocity at the tyre's axle, V_x and tyre's rotational velocity, V_w. The slip ratio, ρ_{ij} value is set to absolute to ensure that the vehicle's wheel slip ratio remains within the tyre-road friction coefficient driving conditions. This is important because when a vehicle corners, the velocity of its inner tyre decreases relative to the vehicle's velocity, resulting in a negative slip ratio. Eq. (4) expresses the slip ratio for acceleration, as driving is the primary focus of this study; thus, the slip ratio during acceleration is considered. Here, the integral i represents the front and rear tyres, while the integral j represents the right and left tyres.

$$\rho_{ij} = \left| \frac{V_{wij} - V_x}{V_x} \right| \tag{4}$$

Eq. (5) to Eq. (8) express the sideslip angle of the front tyre, the sideslip angle of the rear tyre, and the angle formed by the velocity vectors of the front and rear tyres relative to the vehicle's longitudinal axis, denoted as α_f, α_r, θ_{vf}, and θ_{vr}, correspondingly. Eq. (9) and Eq. (10) present the equations for longitudinal and lateral forces, where for front tyres, $\alpha = \alpha_f$ and for rear tyres, $\alpha = \alpha_r$. Conversely, λ is provided by Eq. (11), and the condition for the function of λ, $f(\lambda)$ is expressed in Eq. (12) and Eq. (13). Here, F_z is the vertical force affected by load transfer acting on the tyre, and μ is the tyre-road friction coefficient. Eq. (14) provides the value of μ_{ij} for each tyre, where k is the constant factor for dry road surfaces, which is set to 0.9.

2.3. *Load Transfer Model*

The examination of a vehicle's behaviour during manoeuvres requires consideration of the load distribution at each wheel. The vehicle's free body diagram can be used to estimate the impact of load shifting as shown in **Figure 2a** and **Figure 2b**

$$\alpha_f = \delta - \theta_{vf} \tag{5}$$

$$\alpha_r = -\theta_{vf} \tag{6}$$

$$\theta_{vf} = \tan^{-1}\left(\frac{V_y + l_f\,\dot{\varphi}}{V_x}\right) \tag{7}$$

$$\theta_{vr} = tan^{-1}\left(\frac{V_y - l_f\,\dot{\varphi}}{V_x}\right) \tag{8}$$

$$F_{xij} = C_\sigma \frac{\rho_{ij}}{1 + \rho_{ij}} f(\lambda) \tag{9}$$

$$F_{yij} = C_\alpha \frac{\tan\alpha}{1 + \rho_{ij}} f(\lambda) \tag{10}$$

$$\lambda = \frac{\mu F_z(1 + \rho_{ij})}{2\left[\left(C_\sigma \rho_{ij}\right)^2 + (C_\alpha \tan(\alpha))^2\right]^{1/2}} f(\lambda) \tag{11}$$

$$f(\lambda) = (2 - \lambda)\lambda \quad if\ \lambda < 1 \tag{12}$$

$$f(\lambda) = 1 \quad if\ \lambda > 1 \tag{13}$$

$$\mu_{ij} = -1.05k\left[exp\left(-45\rho_{ij}\right) - exp\left(-0.45\rho_{ij}\right)\right] \tag{14}$$

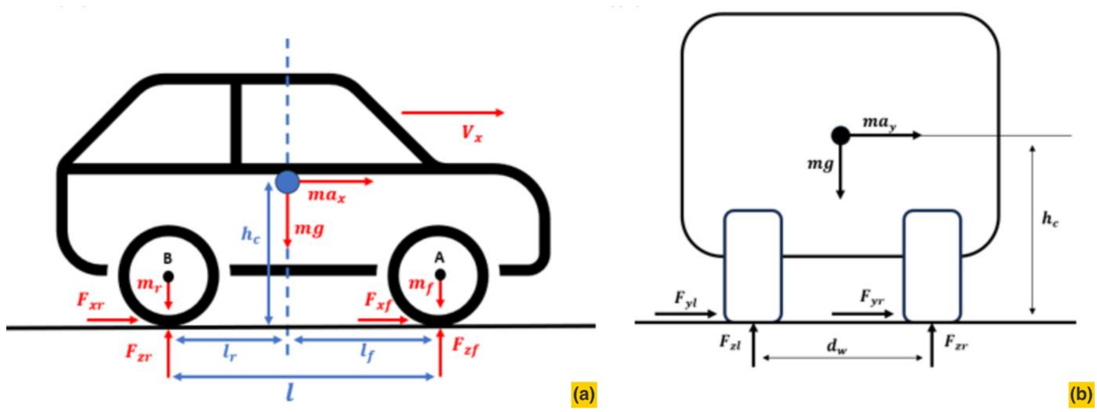

Figure 2. (a) Longitudinal Force and Mass Distribution of the Vehicle and (b) Load Transfer during Lateral Movement

for longitudinal and lateral axes, respectively. The vertical force can be calculated based on the dynamic load at each tyre transferred during manoeuvres due to the existence of longitudinal and lateral acceleration during the occasion [24]. Eq. (15) to Eq. (18) represent the vertical forces at the front right, front left, rear right, and rear left tyres, respectively.

The static mass at each tyre is assumed to be the same, which can be represented as m_{sfl}, m_{sfr}, m_{srr}, and m_{srl} for the front left, front right, rear right, and rear left tyres, respectively. Here, m, l, g, h_c, l_f, l_r, a_x, and a_y represent the mass of the vehicle, the wheelbase, the height from the centre of gravity, the distance between the centre of gravity and the front or rear tyres, longitudinal acceleration, and lateral acceleration, respectively. To simulate an instance of unbalanced overloading, a set of loads, $load_{ij}$ is added to each tyre. h_{cg} and g represent the height from the vehicle's centre of gravity and gravitational acceleration, respectively. In this context, the integral i represents the front and rear tyres, while the integral j represents the right and left tyres. The load is transferred from the left to the right wheel as the vehicle is in the right cornering. This occurs due to the positive lateral acceleration in the right direction, which is generated at the centre of the vehicle body as a result of the driver's steering input. Consequently, the vehicle tends to roll to the right as more weight is transferred to the right wheel. As the vehicle is in the left cornering, the load is transferred to the left wheel, and the vehicle tends to roll to the left. Therefore, the vehicle's stabilisation factor must be considered in the development of the active system, especially when human lives are at stake. However, vehicle stability varies based on the responsiveness of the vehicle's actuator (braking and steering), vehicle dimensions, additional load distribution, and human driving behaviour.

In order to find the mass of the wheel for the rear part, m_r, the moment of inertia at point A, M_A is zero, considering the vehicle is in a static position. Consequently, the results derived from the moment balance are presented in Eq. (19). The mass for the front part of the wheel, m_f of the vehicle can be calculated by assuming that the

$$F_{zfr} = \left(m_{sfr} + load_{ij}\right)g\frac{l_r}{l} + \frac{m_f a_y h_{cg}}{d_w} - ma_x\frac{h_{cg}}{l} \tag{15}$$

$$F_{zfl} = \left(m_{sfl} + load_{ij}\right)g\frac{l_r}{l} - \frac{m_f a_y h_{cg}}{d_w} - ma_x\frac{h_{cg}}{l} \tag{16}$$

$$F_{zrr} = \left(m_{srr} + load_{ij}\right)g\frac{l_f}{l} + \frac{m_r a_y h_{cg}}{d_w} + ma_x\frac{h_{cg}}{l} \tag{17}$$

$$F_{zrl} = \left(m_{srl} + load_{ij}\right)g\frac{l_f}{l} - \frac{m_r a_y h_{cg}}{d_w} + ma_x\frac{h_{cg}}{l} \tag{18}$$

moment of inertia at point B, M_B is also zero, as the vehicle is in a static condition. Eq. (20) represents the method for finding the mass of the front part of the wheel. The masses for both the front and rear parts of the wheel will then be divided by two, corresponding to the number of wheels on each side of the vehicle.

$$\begin{gathered} M_A = l_f mg - l m_r g \\ if\ M_A = 0 \\ m_r = \frac{-\, l_f mg}{lg} \end{gathered} \tag{19}$$

$$\begin{gathered} M_B = l_r mg - l m_f g \\ if\ M_B = 0 \\ m_f = \frac{-\, l_f mg}{lg} \end{gathered} \tag{20}$$

2.4. *Kinematic Model*

Kinematic modelling is the process of developing a mathematical description of a vehicle's motion without considering the forces affecting it. Therefore, the only basis for the mathematical formulas is the geometric relationship of the system. Eq. (21) and Eq. (22) express the longitudinal and lateral velocities, which are denoted as $\dot{X}$ and $\dot{Y}$, respectively, while Eq. (23) and Eq. (24) represent the longitudinal, X and lateral velocities, Y for vehicle displacement in inertial coordinate frames, respectively.

$$\dot{X} = \dot{x}\cos\varphi - \dot{y}\sin\varphi \tag{21}$$

$$\dot{Y} = \dot{x}\sin\varphi + \dot{y}\cos\varphi \tag{22}$$

$$X(t) = \int_0^t \dot{X}(t)dt \tag{23}$$

$$Y(t) = \int_0^t \dot{Y}(t)dt \tag{24}$$

3. Research Methodology

3.1. *Experimental Vehicle and Instrumentation*

The working model for the experimental vehicle is the Malaysian national car, Proton Persona, as shown in **Figure 3**. The vehicle is a sedan equipped with a manual gearbox and a 1.6-L engine. **Table 1** presents the general specifications of the experimental vehicle. Several areas of the vehicle were modified to enable the installation of sensors, a video system, and a data gathering system (DAS). A GPS sensor, model number DEWE-VGPS-200c, was installed in the car to monitor distance, speed, and mileage travelled.

The GPS was installed on top of the car to maximise satellite detection. For the GPS to generate accurate data, it must be able to recognise a minimum of five satellites. The tyre's angular speed was determined using the Kistler's wheel pulse transducer, while the steer wheel angle was measured using an RV4 arm sensor. The tyre angular speed sensor was placed in the centre of the rim, which rotates with 500 pulses. The tyre's angular speed can be multiplied by its radius to calculate the tyre's linear velocity. Nevertheless, in this study, the wheel pulse transducer sensor was only installed on the left side of the wheel.

Simultaneously, the tri-axial gyroscopic sensor was positioned at the vehicle's centre of gravity. The sensor from Xsens Motion Technology (model: MTi and MTx) was used in this experiment. This sensor can measure acceleration and deceleration in three directions: longitudinally, laterally, and vertically. In addition, roll, pitch, and yaw angles can be measured using this sensor. The most relevant data for analysing manoeuvres are the yaw angle

Table 1. Technical specifications of the vehicle

Parameter	Value
Mass of the vehicle, m	1,447.5 kg
Front track, d_{wf}	1.475 m
Rear track, d_{wr}	1.470 m
Length from the front wheel to the centre of gravity, l_f	1.08 m
Length from the rear wheel to the centre of gravity, l_r	1.52 m
Height of the centre of gravity, h_c	0.479 m
Wheel radius, r	0.297 m

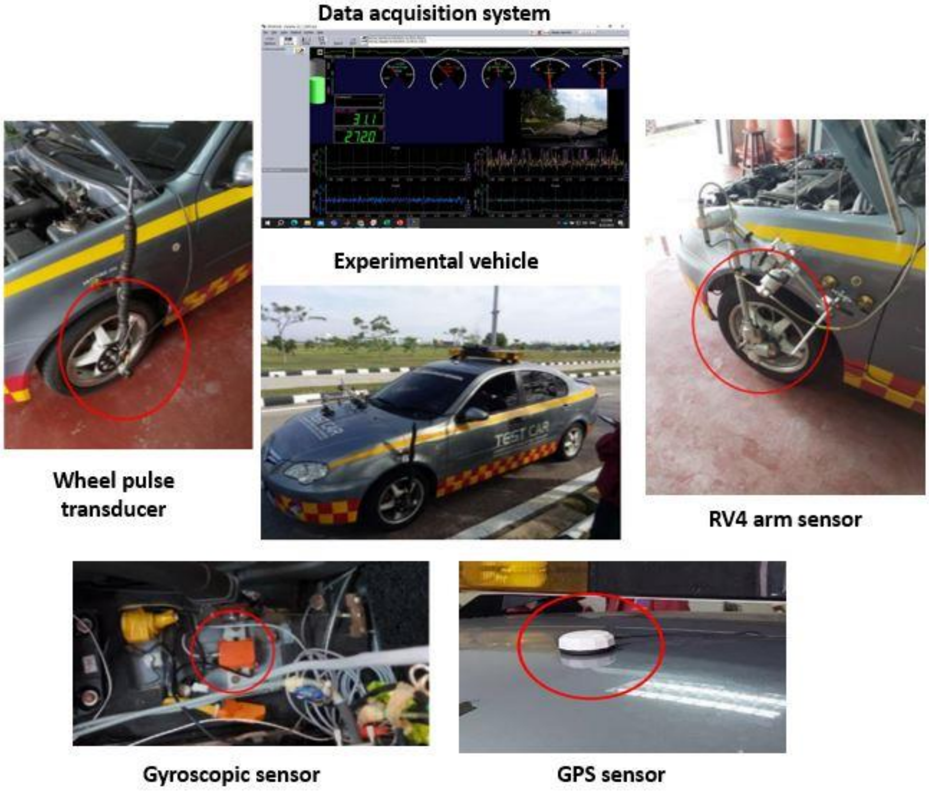

Figure 3. Experimental vehicle and instrumentation

and lateral acceleration, as these parameters can be utilised to ensure that the manoeuvre is smooth during CA.

The DAS was used to collect sensor data at a frequency of 500 Hz. At this frequency, the DAS (model: Dewetron) can record signals from the sensors every 0.002 s. The Dewesoft software is integrated with the DAS for real-time data processing, presentation, and storage. Figure 3 shows the experimental vehicle and the sensors that have been strategically positioned at various locations [30].

3.2. *Experimental Procedure and Scenario*

Traffic control and a test track are essential for the execution of the experiment. The satellite view of the test track at Universiti Malaysia Pahang Al-Sultan Abdullah (UMPSA) is depicted in Figure 4. The CA experiment was carried out on this track, which is closed to other vehicles as a safety precaution, with security personnel overseeing the area. An experienced driver from UMPSA and Automotive Engineering Centre operated the vehicle during the experiment. The data were recorded in the DAS by an assistant officer seated in the back. The maximum vehicle's velocity during the real-time CA experiment was restricted to 50 km/h due to safety considerations, including road width and the safety of both the driver and the assistant officer.

The driver began operating the vehicle after calibrating the sensors. The experiment was conducted on an intact, dry road surface. Figure 5 illustrates the vehicle's behaviour while avoiding an obstacle. The assistant officer in the back seat started collecting data as the speed approached 30 km/h, alerting the driver to maintain that speed. The driver started to manoeuvre as the vehicle approached the obstacle. All collected data collected were verified by the assistant officer before being stored in the DAS. To ensure consistent outcomes, the experiment was conducted five times. Subsequently, MATLAB software was used to filter and denoise the raw data. This step was repeated when the vehicle avoided an obstacle at 40 km/h and 50 km/h. Then, the data of the vehicle's velocity, steer wheel angle, and yaw rate from the experiment were used for system identification of nonlinear vehicle models in simulation, as well as to generate a reference trajectory.

For this experiment, a driving scenario involving a straight road with two lanes and a single stationary obstacle was constructed, as depicted in Figure 5. The width of the road is represented as W_L, and the width of the obstacle is W_v. The length of the obstacle corresponds to L_v. The required parameter values for the CA scenario are tabulated in Table 2. A cone acts as the obstacle in this experiment and is illustrated as a yellow circle in Figure 5.

3.3. System Identification and Reference Trajectory

Figure 6 illustrates the detailed block diagram of the nonlinear vehicle model. The vehicle model, which is a nonlinear model, was calculated using Dugoff's tyre characteristics. As mentioned in the previous subsection, the wheel pulse transducer sensor for measuring wheel velocity was only installed at the front left of the vehicle wheel. To address this limitation, the wheel's velocity model was formulated to obtain the velocity at each wheel. Eq. (25) and Eq. (26) represent the tyre formulation of the front right and front left tyres, respectively, while Eq. (27) and Eq. (28) represent the tyre formulation for the rear right and rear left tyres, respectively.

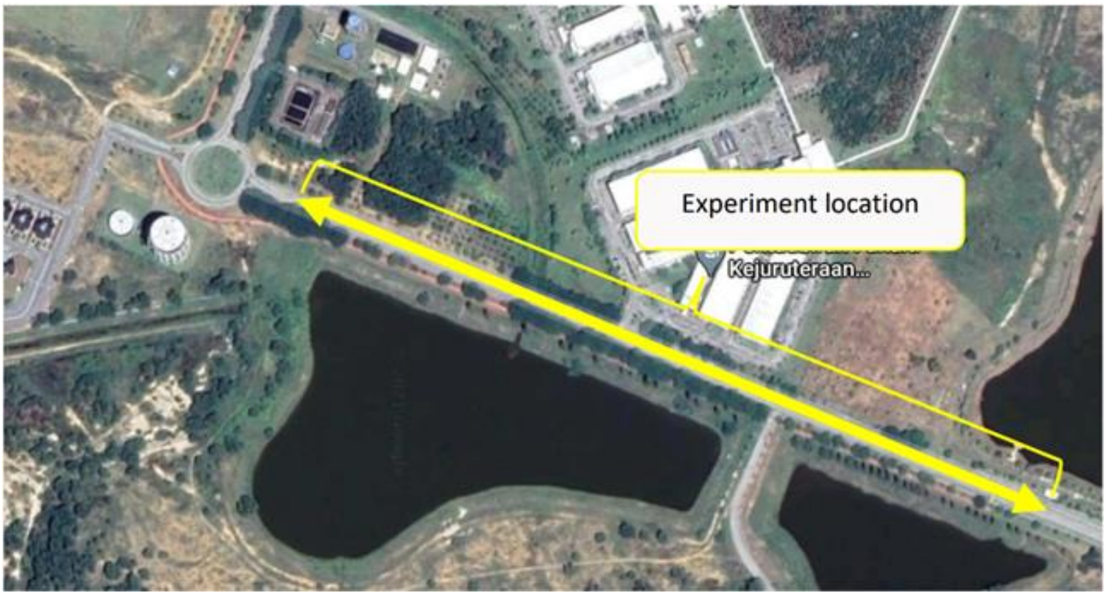

Figure 4. Satellite view of the test track at UMPSA

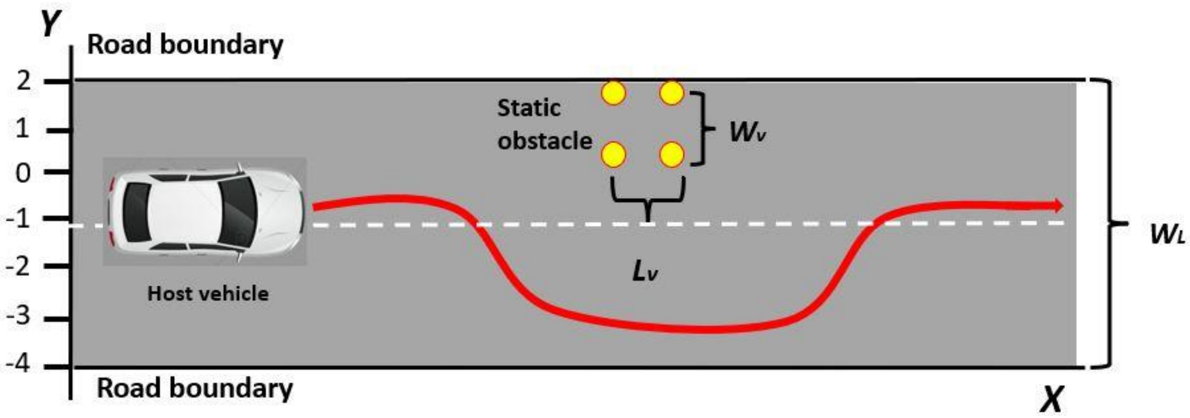

Figure 5. Vehicle's collision avoidance scenario

Table 2. Parameter values for the CA experiment

Label	Parameters	Value
W_v	Width of the obstacle	1.5 m
W_L	Road width	6.0 m
L_v	Length of the obstacle	2.0 m

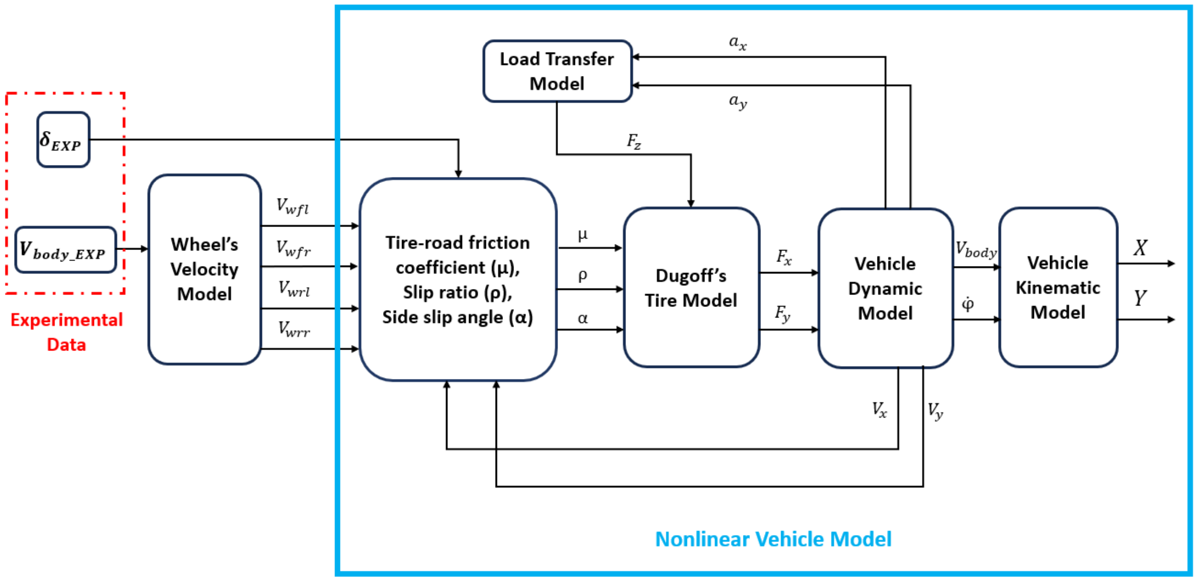

Figure 6. Nonlinear vehicle model

$$V_{wfr} = \left(\dot{x} + \dot{\varphi}\,\frac{d_w}{2}\right)\cos\delta + \left(\dot{y} + \dot{\varphi} l_f\right)\sin\delta \tag{25}$$

$$V_{wfl} = \left(\dot{x} - \dot{\varphi}\,\frac{d_w}{2}\right)\cos\delta + \left(\dot{y} + \dot{\varphi} l_f\right)\sin\delta \tag{26}$$

$$V_{wrr} = \left(\dot{x} + \dot{\varphi}\,\frac{d_w}{2}\right) \tag{27}$$

$$V_{wrl} = \left(\dot{x} - \dot{\varphi}\,\frac{d_w}{2}\right) \tag{28}$$

The experimental vehicle was then used to validate the mathematical vehicle model developed in the earlier phases. By using the same input steering signal while the vehicle travelling at approximately 30 km/h (or 8.333 m/s), the validation process compared the yaw rate measurements of the experimental vehicle with those of the mathematical model. Figure 7 illustrates that the yaw rates for both models are nearly identical when the steering angle input is consistent. Consequently, the nonlinear model is validated. The mean square error for the yaw rate and the vehicle's velocity of the nonlinear model is 0.00091 and 0.049, respectively.

The reference trajectory can be obtained by simulating the nonlinear vehicle model with a wheel velocity model, using the input data from real-time experiments for 30, 40, and 50 km/h, as illustrated in Figure 6. The reference trajectories are depicted in Figure 9 to Figure 11.

3.4. *Simulation Framework for Additional Load Disturbance*

The impact of an additional load on the left and right sides, which acts as a disturbance, was examined to illustrate its effect on the vehicle's trajectory while avoiding an obstacle. The percentage of the vehicle's mass that represents the additional load was used for this calculation. Table 3 presents the vehicle modelling parameters, including the static mass of each wheel, while Table 4 displays the values of the additional load distributed to the vehicle's left and right sides.

The simulation was conducted at speeds of 30, 40, and 50 km/h as the load, $load_{ij}$ was added to the load transfer model, as expressed in Eq. (15) to Eq. (18) for load percentages of 10%, 20%, 30%, and 40%, respectively, at the right side of the vehicle, both at the front and rear. The same procedure was repeated for additional loads at the left side

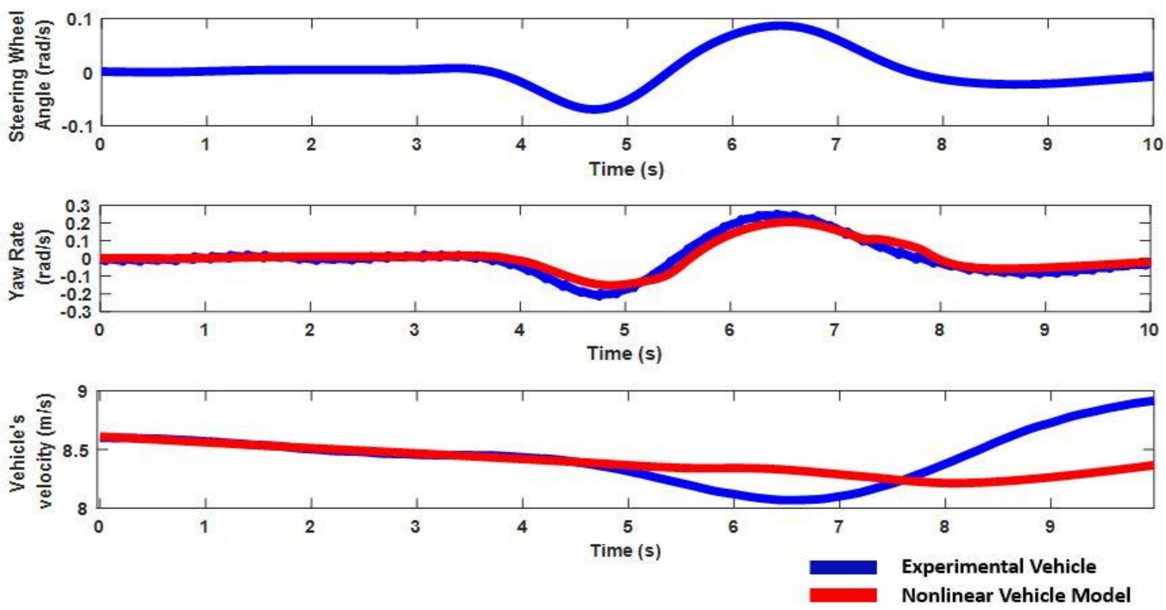

Figure 7. Nonlinear model validation

Table 3. Static mass of each tyre

Label	Parameters	Value
m_{fr}	Static mass of the tyre at the front right	423.12 kg
m_{fl}	Static mass of the tyre at the front left	423.12 kg
m_{rr}	Static mass of the tyre at the rear right	300.63 kg
m_{rl}	Static mass of the tyre at the rear left	300.63 kg

Table 4. Load added distribution on the front and rear sides of the vehicle

Percentage (%)	Total load (kg)	Load at the front side for right and left (kg)	Load at the rear side for right and left (kg)
10	144.75	72.38	72.38
20	289.5	144.75	144.75
30	434.25	217.13	217.13
40	579	289.5	289.5

of the vehicle. In this context, the integral i represents the front and rear, while the integral j represents the right and left sides. Figure 8 illustrates the location of the additional loads applied to the vehicle, specifically on the right and left sides of the wheels. The red rectangle indicates the additional load disturbance on each wheel during the simulation for the CA scenario.

4. Experimental Results for Simulation Analysis

Figure 9 to Figure 11 show the inputs for the nonlinear vehicle model in the simulation. The input for the model consists of the experimental data for the vehicle's velocity and steer wheel angle data collected during CA scenarios while the vehicle travelled at speeds of 30, 40, and 50 km/h. Figure 9a shows that the vehicle's velocity varies from 8.1 m/s to 8.85 m/s, while Figure 9b shows the steer wheel angle approaching its maximum value of 0.085 rad/s. Figure 10a indicates that the vehicle's velocity varies from 10.9 m/s to 11.5 m/s, while Figure 10b depicts the experimental data for the steer wheel angle approaching its maximum value of 0.055 rad/s.

Figure 11a displays the vehicle's velocity ranging from 13.82 m/s to 13.885 m/s, while Figure 11b depicts the experimental data for the steer wheel angle approaching its maximum value of 0.065 rad/s. Human driving is crucial in determining the maximum steer wheel angle of a vehicle while avoiding an obstacle. Figure 9b indicates that the highest maximum steer wheel

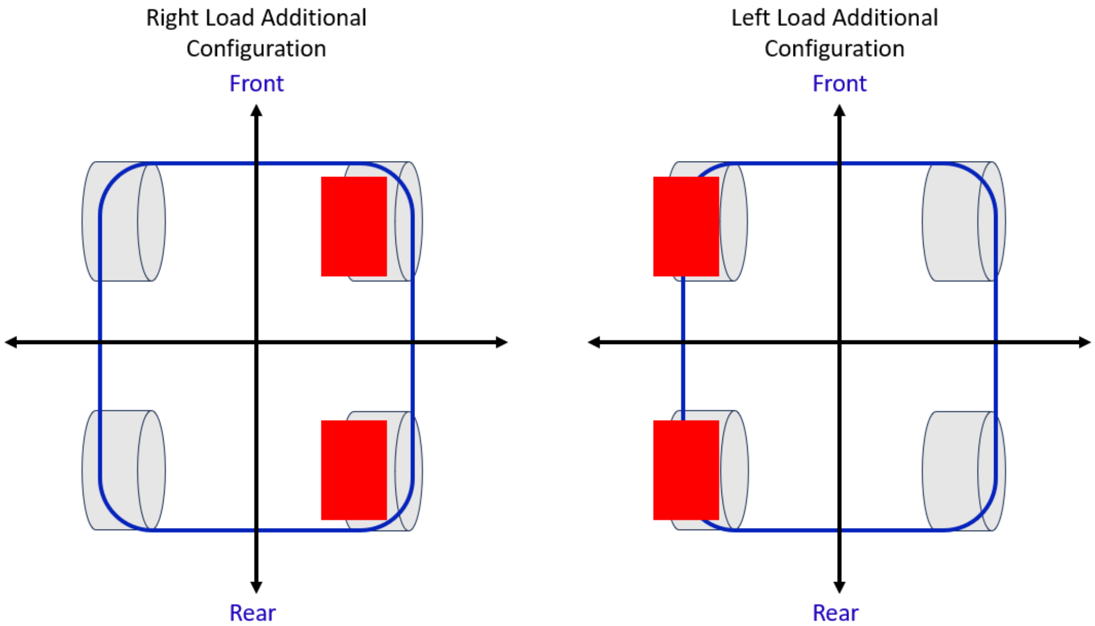

Figure 8. Additional load distribution disturbance

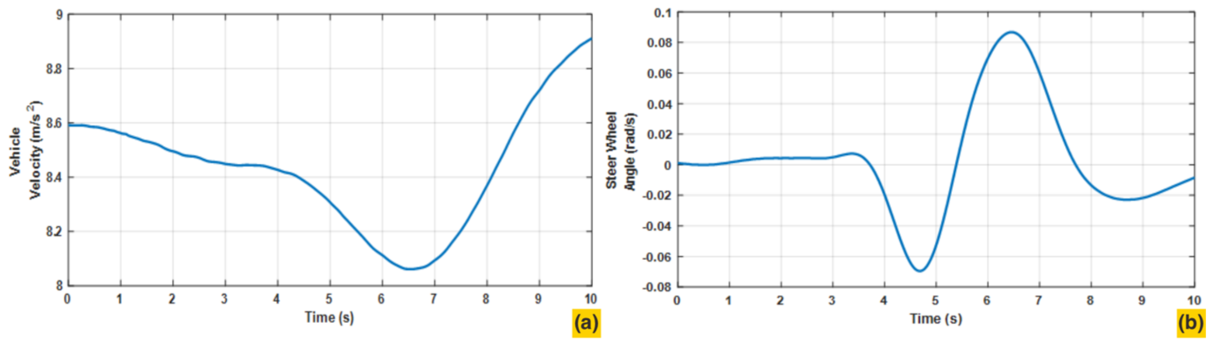

Figure 9. Vehicle's velocity and steer wheel angle experimental data estimated at 30 km/h (8.33 m/s)

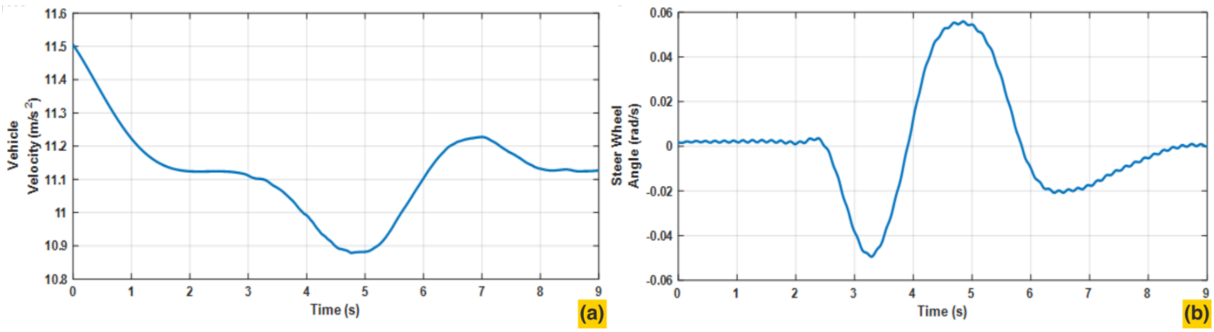

Figure 10. Vehicle's velocity and steer wheel angle experimental data estimated at 40 km/h (11.11 m/s)

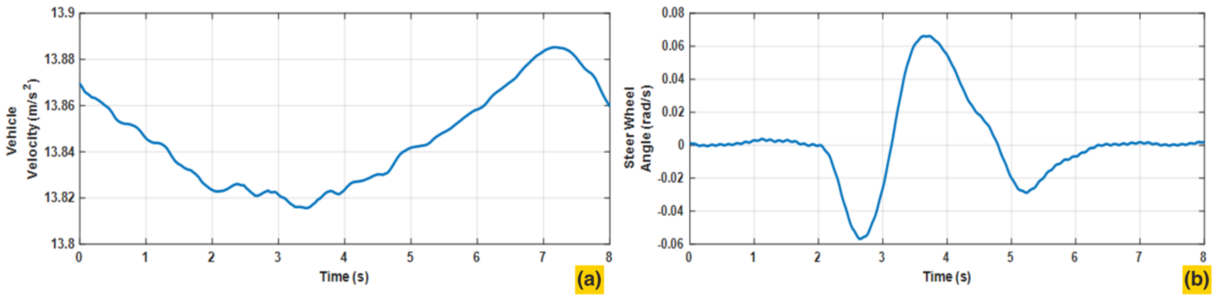

Figure 11. Vehicle's velocity and steer wheel angle experimental data estimated at 50 km/h (13.89 m/s)

angle occurs when the vehicle travels at approximately 30 km/h, in comparison to 40 km/h and 50 km/h. However, a lower vehicle velocity does not necessarily guarantee a higher maximum steer wheel angle of the vehicle. It can be demonstrated that the steer wheel angle of the vehicle while avoiding an obstacle at around 50 km/h is higher than that at 40 km/h. Generally, the vehicle's velocity changes significantly when the driver manoeuvres the vehicle during a CA scenario. **Figure 9a**, **Figure 10a** and **Figure 11a** show the significant changes in the vehicle's velocity at around 3.5–10 s, 2.5–8 s, and 2–6.5 s when the vehicle travels at approximately 30, 40, and 50 km/h, respectively.

5. Effect of Additional Load Disturbance on Vehicle Dynamics while Avoiding an Obstacle

This chapter focuses on analysing the effect of additional load disturbances on the vehicle in a CA scenario. Subsections 5.1, 5.2, and 5.3 elaborate on the dynamic behaviour of the vehicle, especially regarding the normal force, acceleration in the y-direction, and yaw rate, which are affected by disturbances as the vehicle travels at speeds of 30, 40, and 50 km/h. This chapter also discusses the vehicle's trajectory for each velocity in relation to the vehicle's dynamic behaviour. In each subsection corresponding to 5.1, 5.2, and 5.3, the normal force can be categorised as no load, 10%, 20%, 30%, and 40%, represented by blue, red, yellow, purple, and green lines, respectively, for additional load disturbances at the right and left sides of the wheels. The lateral acceleration and yaw rate of the vehicle are represented by blue, red, yellow, purple, and green lines, which correspond to no load, 10%, 20%, 30%, and 40% additional load disturbances for the right and left sides of the wheels.

5.1. *Velocity = 30 km/h*

Figure 12 and **Figure 13** illustrate the effect of additional load disturbances at the right and left wheels for the normal force acting on each wheel, respectively. The significant changes in the normal force at each wheel correspond to the additional load placement. For example, **Figure 12** shows a huge difference in the normal force at the front right and rear right wheels due to the additional load placed at the right side of the vehicle. When the vehicle steers to the left before exiting the lane from 4 s to 4.6 s, the load from the left side transfers to the right side of the wheel. During this period, the normal force at the left side of the wheel experiences a significant decrease, while the normal force at the right side of the wheel increases. As the vehicle manoeuvres to the right to exit the lane from 4.6 s to 6.5 s, the total load at the right side transfers to the left side of the wheel. The normal force at the left side of the wheel experiences a significant increase, while the normal force at the right side of the wheel decreases during this phase. Next, as the vehicle steers to the left side to re-enter the lane from 6.5 s to 8 s, the normal force at the right side of the wheel increases, while the normal force at the left side decreases. The vehicle then slightly steers to the right to stabilise its position, allowing it to return to the lane between 8 and 9 s. This is indicated by an increase in the normal force at the left side of the wheel and a decrease at the right side, showing that the load at the right side of the vehicle shifts to the left side throughout this time period. Once the vehicle returns to the initial lane and travels without input from steering (deg = 0°), the normal forces on both sides of the wheel return to their initial values. **Figure 12** illustrates how an increase in the additional load disturbance percentage at the right side of the wheel significantly affects the normal force acting on each wheel.

Figure 13 shows the varying values of normal force with increasing additional load percentages at the left side, which influence the normal force at the front left and rear left of the wheel. The load from the left side shifts to the right side of the wheel when the vehicle steers to the left before exiting the lane between 4 and 4.6 s. The normal force on the left side of the wheel decreases significantly during this period, while the normal force on the right side of the wheel increases. The weight on the right side of the wheel shifts to the left side as the vehicle moves to the right before exiting the lane between 4.6 and 6.5 s. In this period, there is a noticeable increase in the normal force at the left side of the wheel and a decrease at the right. The normal force at the right side of the wheel subsequently increases while the normal force at the left side of the wheel decreases as the vehicle steers to the left to re-enter the lane, commencing from 6.5 s to 8 s. Next, from 8 s to 9 s, the vehicle steers slightly to the right to stabilise its position before re-entering the lane. As the normal force at the left side of the wheel increases and the right side of the wheel experiences a decrease, the load at the right side of the vehicle is transferred to the left side throughout this time phase. The normal forces on both sides of the wheel return to their starting value once the vehicle moves back into its original lane and without steering input (deg = 0°). **Figure 13** illustrates how an increase in the additional load disturbance percentage at the right side of the wheel significantly affects the normal force acting on each wheel.

Figure 14 and **Figure 15** show the behaviour of the vehicle's lateral acceleration and yaw rate during the CA scenario by incorporating additional load disturbances at the right and left sides of the wheels, respectively. The significant changes in lateral acceleration and yaw rate can be classified into five phases: (1) the vehicle steers left before exiting the lane from 4 s to 4.6 s, (2) the vehicle steers to the right to exit the lane from 4.6 s to 6.5 s, (3) the vehicle steers to the left to re-enter the

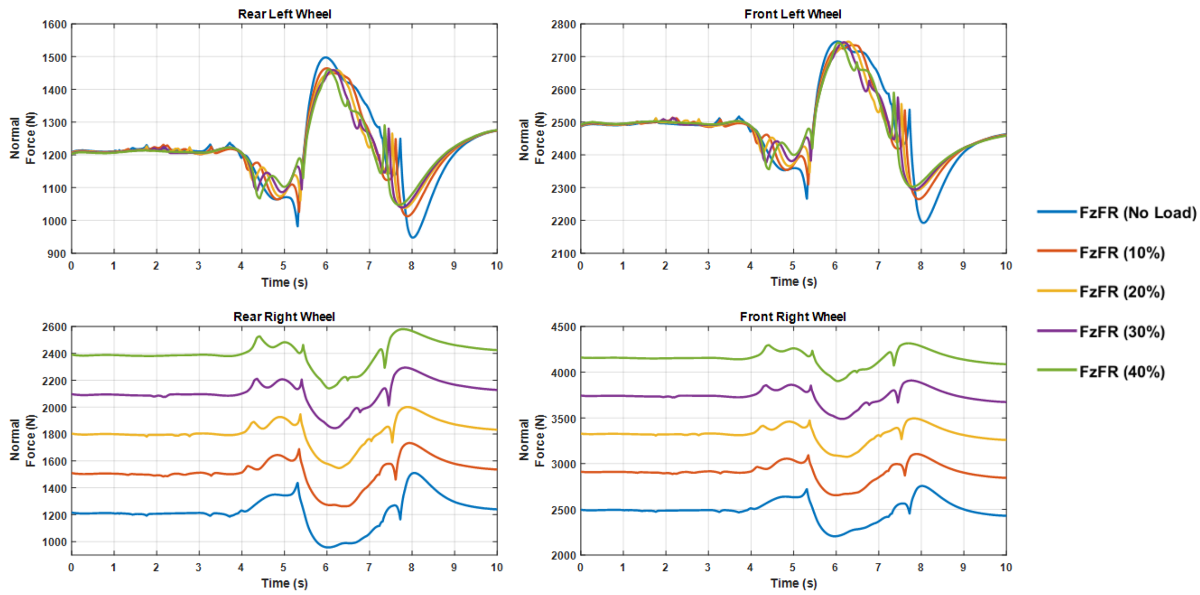

Figure 12. Normal force at each wheel corresponding to additional load disturbance at the right wheel for V = 30 km/h

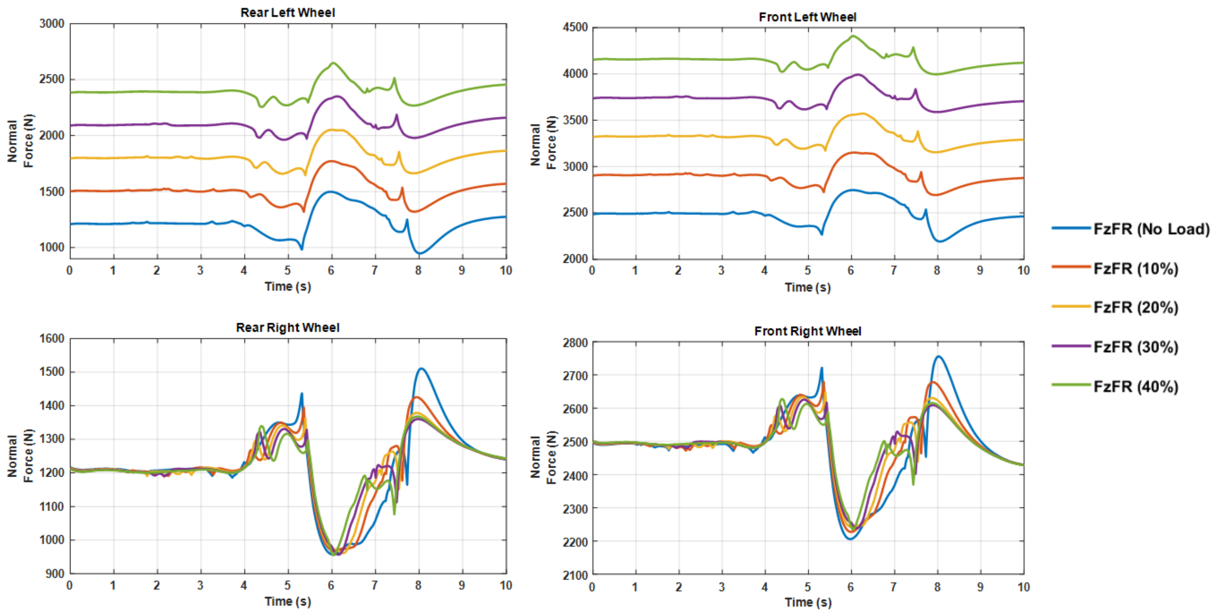

Figure 13. Normal force at each wheel corresponding to additional load disturbance at the left wheel for V = 30 km/h

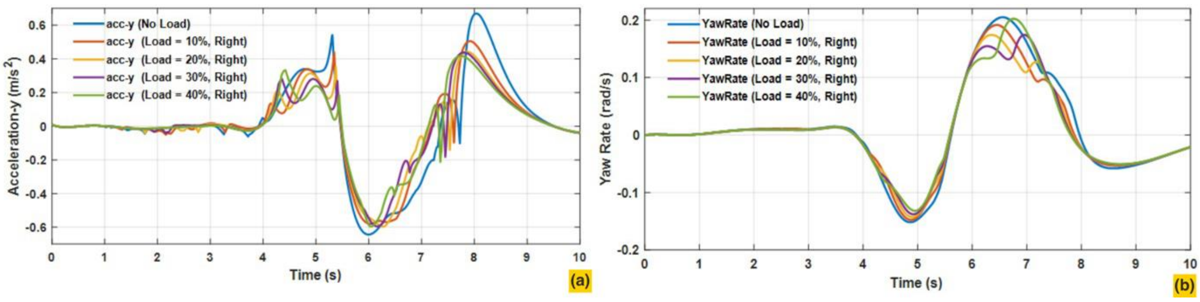

Figure 14. Effect of additional load disturbance at the right wheel of the vehicle for V = 30 km/h: (a) Lateral acceleration of the vehicle and (b) Yaw rate of the vehicle

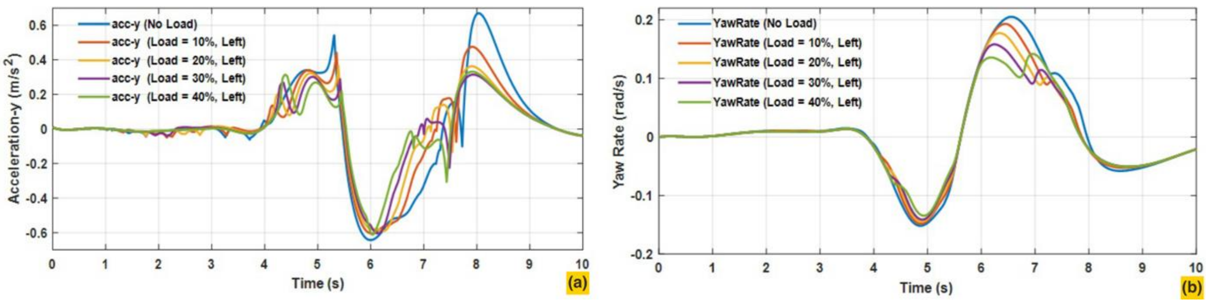

Figure 15. Effect of additional load disturbance at the left wheel of the vehicle for V = 30 km/h: (a) Lateral acceleration of the vehicle and (b) Yaw rate of the vehicle

initial lane from 6.5 s to 8 s, (4) the vehicle steers to the right slightly to stabilise its position from 8 s to 9 s, and (5) the vehicle is in its initial lane from 9 s to 10 s. Phases 1 until 4 demonstrate the effect of the initial load and the increasing additional load shifting to the opposite side of the vehicle's trajectory and lateral acceleration. Phase 1 shows that the lateral acceleration of the no-load condition is higher compared to other conditions due to the effect of load shifting from the left side to the right side of the wheel. Phase 2 illustrates that the lateral acceleration in the right direction and the yaw rate of the vehicle with additional load percentage are reduced compared to the no-load condition, as the additional load shifts from the right to the left side. Phase 3 visualises that once the vehicle steers to the left, the effect from the previous phase still influences the lateral acceleration, especially at 40% additional load, until the vehicle reaches 7.8 s. During this time, the load from the left wheel, without any additional load transfer to the right side, significantly reduces compared to the no-load condition. The vehicle's yaw rate also exhibits a significant difference between the additional load percentages and the no-load condition, especially at 40% and 30% additional load at the left wheels. Phase 4 shows that as the vehicle turns slightly to the right, the effect of load shifting from the right to the left reduces both lateral acceleration and yaw rate compared to the no-load condition. Phase 5 indicates that there is no difference in lateral acceleration and yaw rate between the additional load percentages and the no-load condition as the vehicle travels in a straight line.

Figure 16 illustrates the trajectory of the vehicle travelling at approximately 30 km/h. The black dotted line represents the reference trajectory of the vehicle without any additional load transfer phenomena while avoiding an obstacle. An obstacle is represented by a yellow rectangle with red dotted lines. The vehicle trajectories, when an additional load of 10% is applied at the right and left sides of the wheels, show minimal changes compared to the reference trajectory, as indicated by the turquoise line and blue dotted line, respectively. The vehicle experiences significant oversteer and slight understeers from 50 m to 69 m and from 72 m to 80 m, respectively, for a 10% additional load at both sides of the wheels. Next, the vehicle's trajectories begin to deviate more from the ideal reference trajectories as the load increases to 20% at the right and left wheels, as shown by the orange line and chocolate dotted line, respectively. The vehicle experiences significant oversteer in its trajectory for both sides of the wheels from 50 m to 68 m. Subsequently, the vehicle experiences significant understeer starting

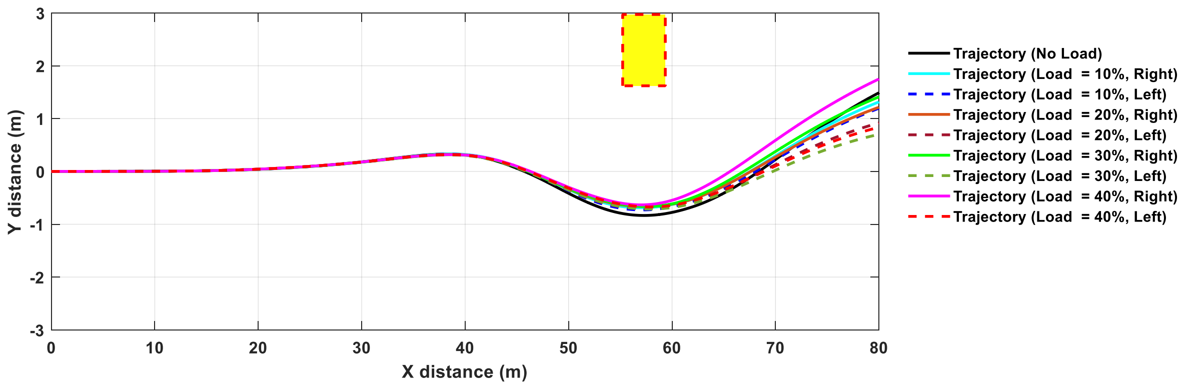

Figure 16. Vehicle's trajectories with additional load at 30 km/h

from 69 m to 80 m for a 20% additional load at both sides of the wheels. The dark green dotted line represents a 30% load at the left wheel, illustrating significant oversteer from 50 m to 65 m and high understeer from 68 m to 80 m. The green line indicates a 30% additional load at the right wheel, showing high oversteer from 50 m to 70 m. The pink line depicts a vehicle's trajectory that deviates significantly, experiencing significantly high oversteer for a 40% additional load at the right, starting from 50 m to 80 m. The red dotted line represents a 40% additional load at the left side of the wheel, demonstrating significant oversteer and understeer occurring from 50 m to 65 m and from 70 m to 80 m, respectively. The deviation of the trajectories begins to increase as the vehicle manoeuvres past the obstacle, as shown in Figure 16. The vehicle successfully avoids an obstacle and does not collide with the road divider for all additional load percentages for the right and left sides of the wheels while travelling at approximately 30 km/h.

5.2. Velocity = 40 km/h

The effects of additional load disturbances at the right and left wheels for the normal force applied on each wheel are shown in Figure 17 and 18, respectively. The additional load location corresponds to the notable changes in the normal force at each wheel. For instance, Figure 17 illustrates that a greater load positioned on the right side of the vehicle causes a significant variation in the normal force at the front right and rear right of the wheels. The load from the left side shifts to the right side of the wheel when the vehicle steers to the left before exiting the lane between 2.5 and 3.3 s. The normal force on the left side of the wheel significantly decreases throughout this time, while the normal force on the right side of the wheel increases. The entire weight on the right side of the wheel shifts to the left as the vehicle moves to the right, exiting the lane between 3.4 and 5.2 s. During this period, there is a noticeable increase in the normal force at the left side of the wheel and a decrease at the right. Subsequently, the normal force at the right side of the wheel increases, while the normal force at the left side of the wheel decreases as the vehicle steers to the left to re-enter the lane, beginning at 5.2 s and ending at 6.2 s. Then, the vehicle steers to the right slightly to stabilise the vehicle's position for re-entering the lane from 6.3 s to 7.2 s. During this phase, the load at the right side of the vehicle is transferred to the left side of the vehicle, as indicated by an increase in the normal force at the left side of the wheel, while at the right side of the wheel experiences a decrease in normal force. Once the vehicle returns to the initial lane and travels without any input from steering (deg = 0°), the normal forces for both sides of the wheels return to their initial value. Figure 17 illustrates that an increase in the additional load disturbance percentage at the right side of the wheel significantly affects the normal force acting on each wheel.

Figure 18 illustrates how the normal force at the front left and rear left of the wheel varies significantly due to the larger load positioned on the left side of the vehicle. When the vehicle turns left prior to exiting the lane at 2.5–3.3 s, the load from the left side shifts to the right side of the wheel. During this period, the normal force on the right side of the wheel increases, while the normal force on the left side of the wheel decreases significantly. Between 3.4 and 5.2 s, the vehicle manoeuvres to the right to exit the lane, shifting all of the weight from the right side of the wheel to the left. The normal force at the left side of the wheel increases noticeably during this time, while the normal force at the right decreases noticeably. As the vehicle steers to the left to rejoin the lane, starting at 5.2 s and ending at 6.2 s, the normal force at the right side of the wheel increases, while the normal force at the left side of the wheel drops. The vehicle then steers slightly to the right to steady its position so that it can return to the lane between 6.3 and 7.2 s. As shown by an increase in the normal force at the left side of the wheel and a decrease at the right, the load at the right side of the vehicle shifts to the left side throughout this time phase. The normal forces on both sides of the wheels return to their starting value once the vehicle moves back into its original lane and without any steering input (deg = 0°). **Figure 18** illustrates how an increase in the additional load disturbance percentage at the left side of the wheel significantly affects the normal force acting on each wheel.

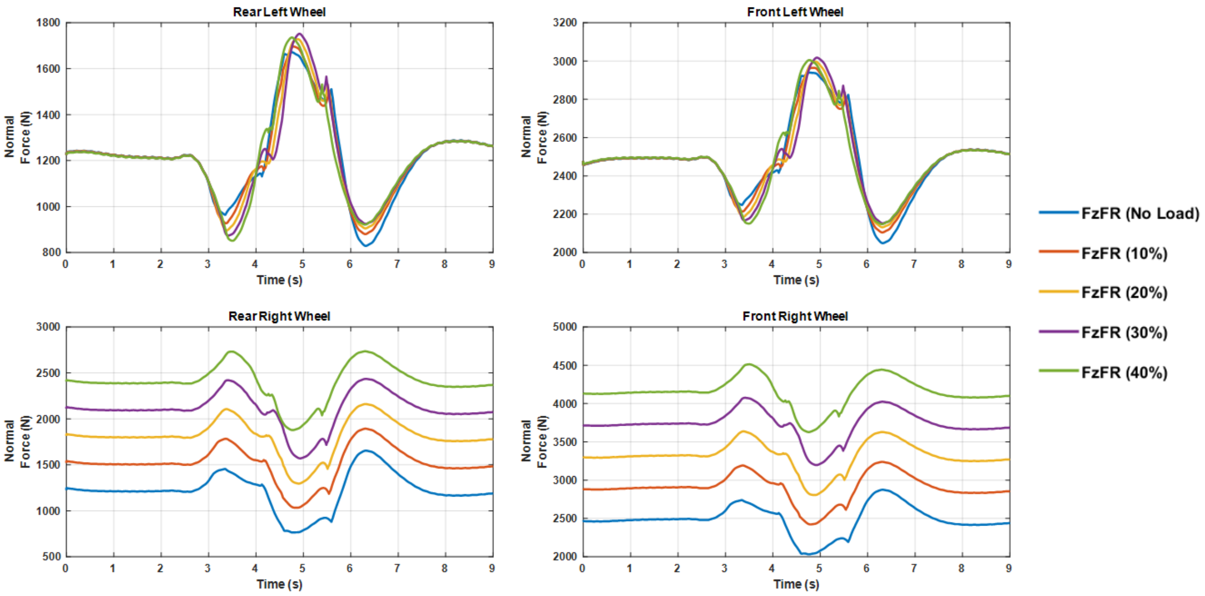

Figure 17. Normal force at each wheel corresponding to additional load disturbance at the right wheel for $V = 40$ km/h

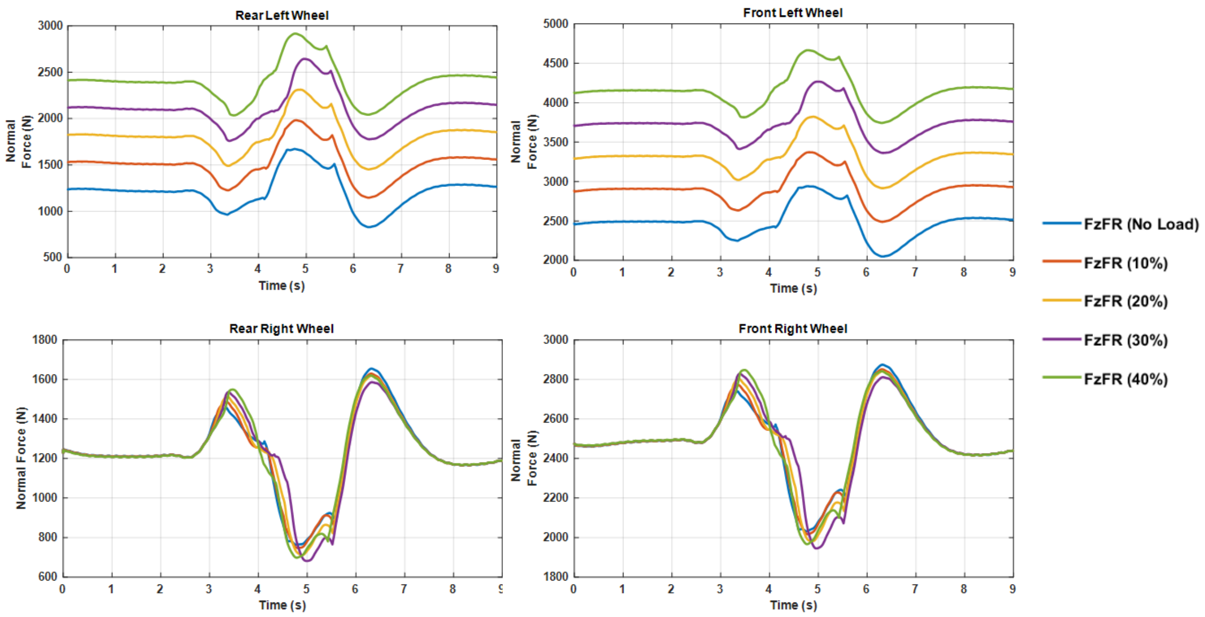

Figure 18. Normal force at each wheel corresponding to additional load disturbance at the left wheel for $V = 40$ km/h

Figure 19 and Figure 20 illustrate the behaviour of the vehicle's yaw rate and lateral acceleration in CA scenarios when the right and left wheels are subjected to additional load disturbances, respectively. The notable variations in lateral acceleration and yaw rate can be divided into five stages: (1) the vehicle steers left before exiting the lane from 2.6 to 3.2 s, (2) the vehicle steers right to leave the lane from 3.2 to 5.2 s, (3) the vehicle steers left to enter the initial lane from 5.2 to 6.4 s, (4) the vehicle steers slightly to the right to stabilise its position from 6.4 to 7.8 s, and (5) the vehicle stays in the initial lane from 7.8 to 9 s. The effects of the initial load and increasing additional load transfer to the opposite side of the vehicle's trajectory and lateral acceleration are visualised in Phases 1 through 4. Phase 1 demonstrates that, due to the initial installation of higher load percentages at either side of the wheel, the lateral acceleration of the no-load condition is lower than that of other conditions. As a result of greater weight moving from the right to the left, Phase 2 demonstrates the vehicle's yaw rate and lateral acceleration to the right when compared to the no-load condition, until it reaches 4.6 s. During this time, the driver counters the steering to the left direction in preparation for the vehicle to re-enter the lane. The time range from 4.4 s to 5.2 s shows a significant load transfer from the left to the right side of the vehicle due to the driver's harsh steer. The harsh steer from the driver is also a main component for the load transfer phenomena to occur. Figure 10b illustrates the pattern of the steer wheel input data from the driver at a velocity of 40 km/h. Specifically, Phase 1 shows unaggressive steer compared to Figure 9b when the vehicle travels at approximately 30 km/h. Phase 3 visualises that once the vehicle steers to the left, the effect from the previous phase still influences lateral acceleration. Due to the aggressive steer from the driver in Phase 3, a significant load transfer effect can be seen throughout this phase from the left to the right, which significantly reduces the value compared to the no-load condition for lateral acceleration, as well as the yaw rate. There is no significant difference in lateral acceleration and yaw rate for the no-load condition compared with additional load percentages due to the small amount of steering initiated by the driver throughout Phase 4. As the vehicle travels in a straight path, Phase 5 demonstrates that there is no difference between additional load percentages with the no-load condition for lateral acceleration and yaw rate.

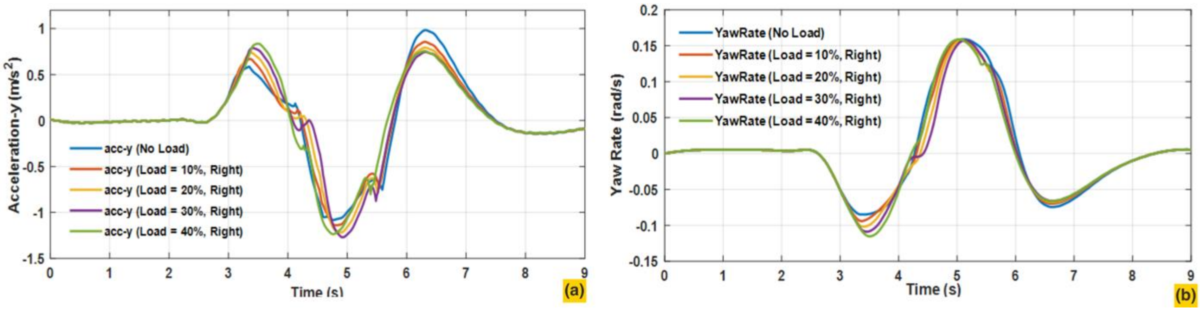

Figure 19. Effect of additional load disturbance at the right wheel of the vehicle for V = 40 km/h: (a) Lateral acceleration of the vehicle and (b) Yaw rate of the vehicle

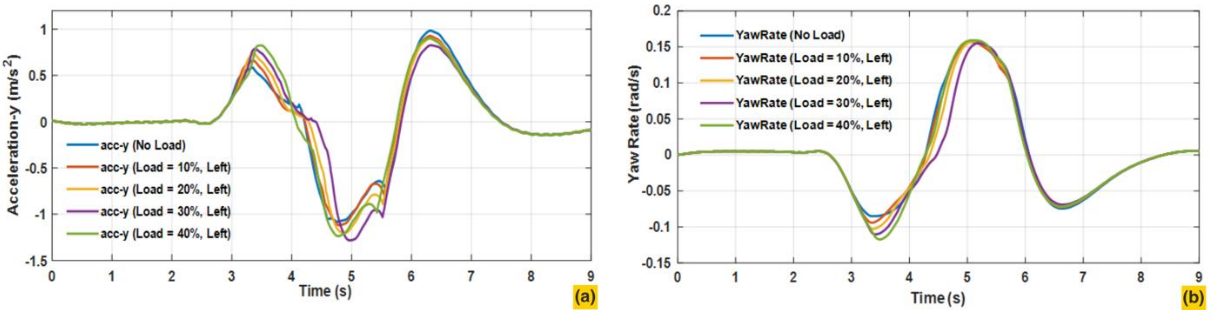

Figure 20. Effect of additional load disturbance at the left wheel of the vehicle for V = 40 km/h: (a) Lateral acceleration of the vehicle and (b) Yaw rate of the vehicle

Figure 21 represents the trajectory of the vehicle when travelling at 40 km/h. The yellow rectangle with red dotted lines indicates an obstacle, while the reference trajectory of the vehicle, without any additional load, is represented by black dotted lines. The vehicle trajectories, as indicated by the blue dotted line and turquoise line, reveal that there is a significant deviation from the reference trajectory, especially when an additional 10% load is applied at the right side compared to the left side of the wheel. The significant understeer can be seen at the right wheel as the vehicle travels at 70 m to 100 m compared to the left wheel. As the load increases to 20% at the right and left wheels, as indicated by the orange line and chocolate dotted line, respectively, the vehicle's trajectories begin to diverge further from the ideal reference trajectories. The 20% additional load at the right wheel results in huge understeer compared to the left wheel when the vehicle travels at 55 m to 100 m. The vehicle experiences tremendous understeer when a 30% additional load is added, especially at the left wheel compared to the right wheel as the vehicle travels from 55 m to 100 m. There is a substantial difference between the 30% load at the left wheel and the 30% load at the right wheel, as indicated by the dark green dotted line and the green line, respectively. The pink line and the red dotted line represent a 40% additional load at the right and left wheels, respectively. Significant understeer occurs for the 40% additional load at both wheels compared to the 30% additional load for both wheels, starting from 45 m to 65 m. This phenomenon shows how the vehicle's trajectory changes when subjected to 40% additional load, which drastically reduces the understeer effect as the vehicle travels from 65 m to 100 m compared to 30% additional load. When the vehicle begins to manoeuvre to avoid an obstacle, the deviation trajectories for all loads begin to deviate from the reference trajectories. As the vehicle manoeuvres past the obstacle, the trajectory deviation increases further. All trajectories at all additional load percentages show that the vehicle experiences understeer while avoiding the obstacle. The understeer phenomenon can be categorised into two stages: (1) the position of the vehicle parallel to the obstacle, and (2) the position of the vehicle when entering the initial lane. The vehicle successfully avoids colliding with the road divider for all additional load percentages on both the right and left wheels while travelling at approximately 40 km/h.

5.3. *Velocity = 50 km/h*

Figure 22 and Figure 23 illustrate the effects of additional load disturbances at the right and left wheels, respectively, with a normal force applied to each wheel. The significant variations in the normal force at each wheel are correlated with the additional load placement. For example, Figure 22 shows how the normal force at the front right and rear right of the wheels varies considerably due to the larger load positioned on the right side of the vehicle. When the vehicle steers to the left before exiting the lane in 2.2–2.8 s, the load from the left side shifts to the right side of the wheel. During this period, the normal force on the right side of the wheel increases, while the normal force on the left side of the wheel decreases. Between 2.9 and 3.9 s, the vehicle turns to the right to exit the lane, shifting all of the weight on the right side of the wheel to the left. The normal force at the left side of the wheel increases significantly during this period, while the normal force at the right decreases noticeably. The vehicle then turns left to rejoin the lane, starting at 4.0 s and ending at 5.5 s,

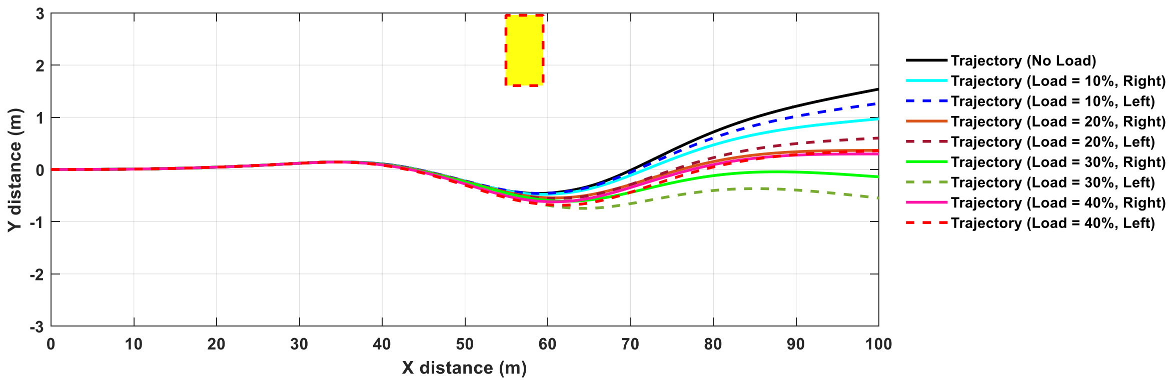

Figure 21. Vehicle's trajectories with additional load at 40 km/h

during which the normal force at the right side of the wheel increases and the normal force at the left side of the wheel decreases. The vehicle then steers slightly to the right to steady its position, allowing it to return to the lane between 5.5 and 6.7 s. As the normal force at the left side of the wheel increases and the right side of the wheel experiences a decrease, the weight from the right side of the vehicle is transferred to the left side of the vehicle throughout these time intervals. After the vehicle returns to the initial lane and without any steering input (deg = 0°), the normal forces on both wheels return to their starting value. **Figure 22** illustrates how an increase in the additional load disturbance percentage at the right side of the wheel significantly affects the normal force acting on each wheel.

Figure 23 illustrates how the greater load position on the left side of the vehicle results in a substantial difference in the normal force at the front left and rear left of the wheels. The load from the left side of the wheel shifts to the right side when the vehicle makes a left turn and leaves the lane in 2.2–2.8 s. The normal force on the right side of the wheel increases throughout this period, while the normal force on the left side decreases. All the weight on the right side of the wheel transfers to the left as the vehicle turns to the right and leaves the lane within 2.9 and 3.9 s. During this period, there is a noticeable increase in the normal force at the left side of the wheel and an obvious decline at the right. The normal force at the right side of the wheel increases and the normal force at the left side of the wheel decreases as the vehicle rotates to the left to re-enter the lane, starting at 4.0 s and ending at 5.5 s. In order to stabilise its position and return to the lane in 5.5–6.7 s, the vehicle then drifts slightly to the right. Throughout these phases, the load transported at the right side of the vehicle is transferred to the left side as the normal force at the left side of the wheel increases and the right side of the wheel declines. The normal forces on both wheels return to their initial value when the vehicle returns to the first lane and without any steering input (deg = 0°). An increase in the extra weight disturbance percentage at the left side of the wheel significantly affects the degree of normal force exerted on each wheel, as shown in **Figure 23**.

Figure 24 and **Figure 25** show how the yaw rate and lateral acceleration of the vehicle respond to additional load disturbances on the left and right wheels, respectively, in CA scenarios. There are five distinct phases in the observable changes in yaw rate and lateral acceleration: (1) the vehicle steers to the left before exiting the lane between 2.2 and 2.8 s, (2) the vehicle steers to the right between 2.9 and 3.9 s, (3) the vehicle steers left to enter the initial lane from 4.0 to 5.5 s, (4) the vehicle steers slightly to the right to stabilise its position from 5.5 to 6.7 s, and (5) the vehicle stays in the initial lane from 6.7 to 8 s. Phases 1 through

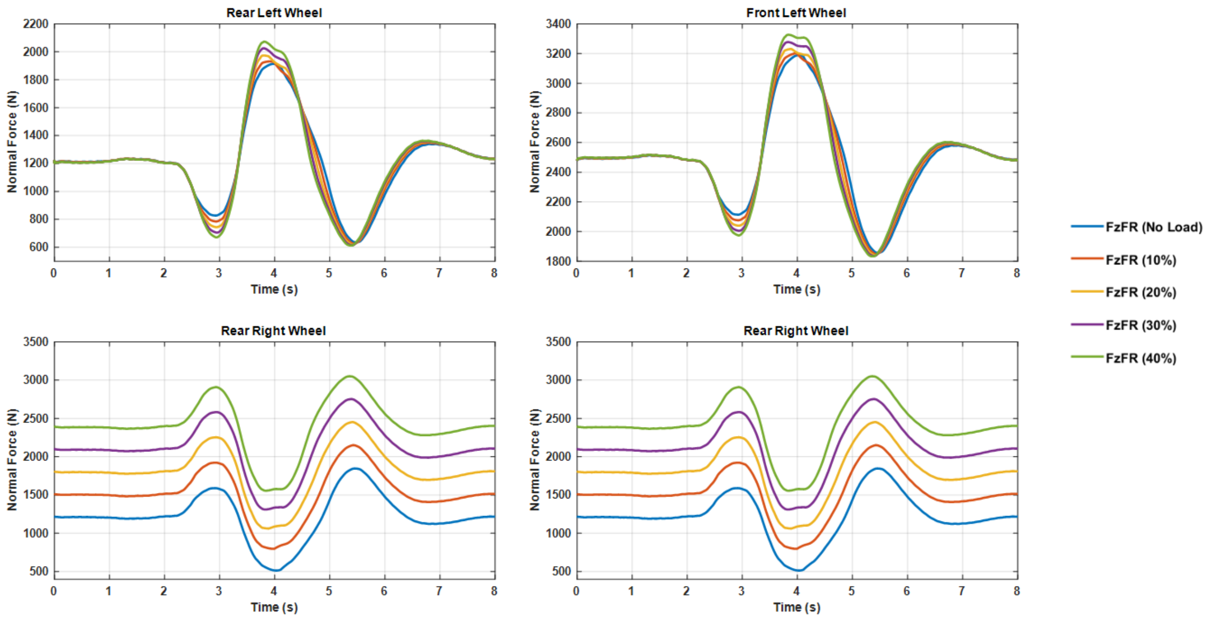

Figure 22. Normal force at each wheel corresponding to additional load disturbance at the right wheel for V = 50 km/h

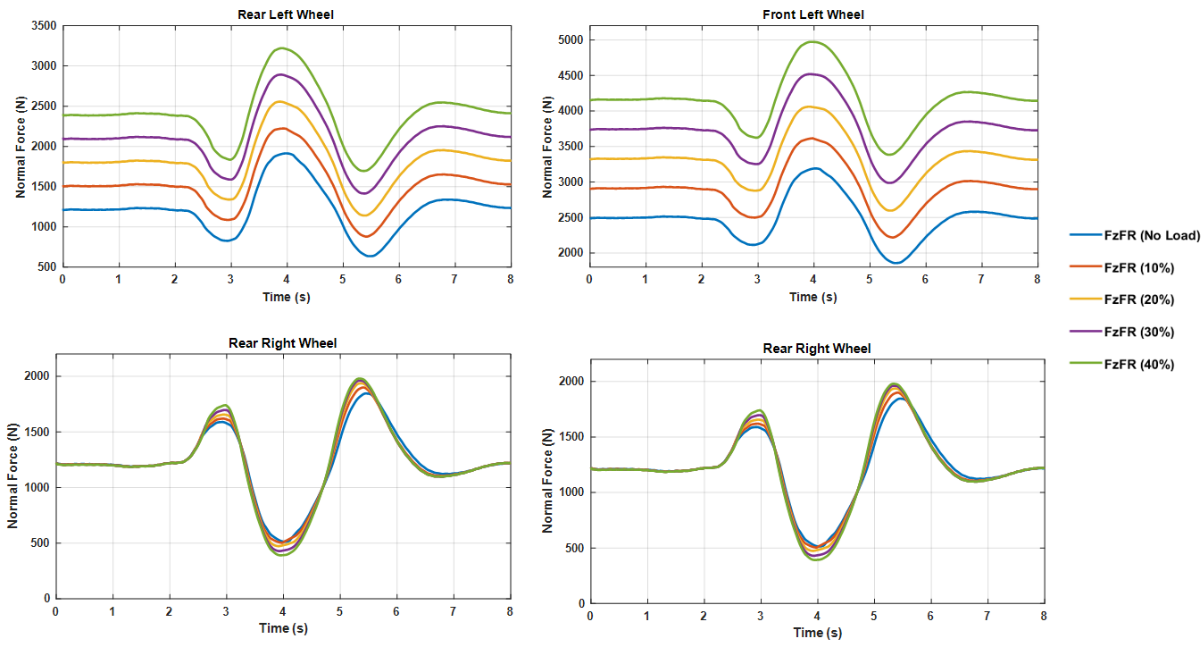

Figure 23. Normal force at each wheel corresponding to additional load disturbance at the left wheel for $V = 50$ km/h

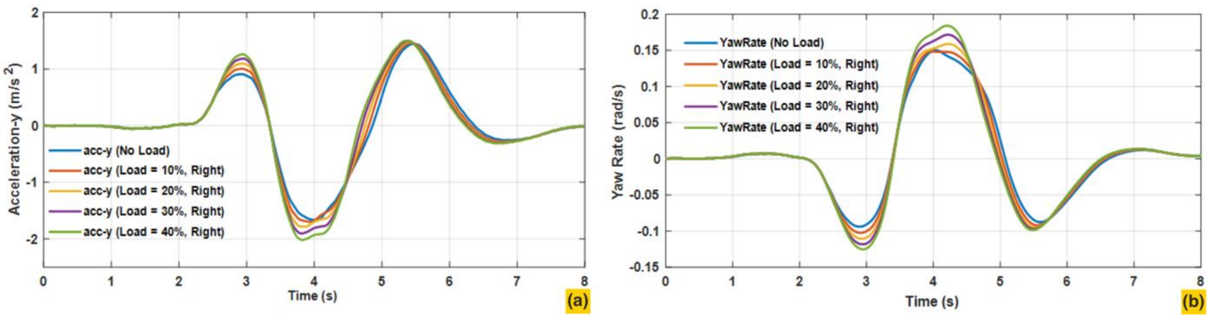

Figure 24. Effect of additional load disturbance at the right wheel of the vehicle for $V = 50$ km/h: (a) Lateral acceleration of the vehicle and (b) Yaw rate of the vehicle

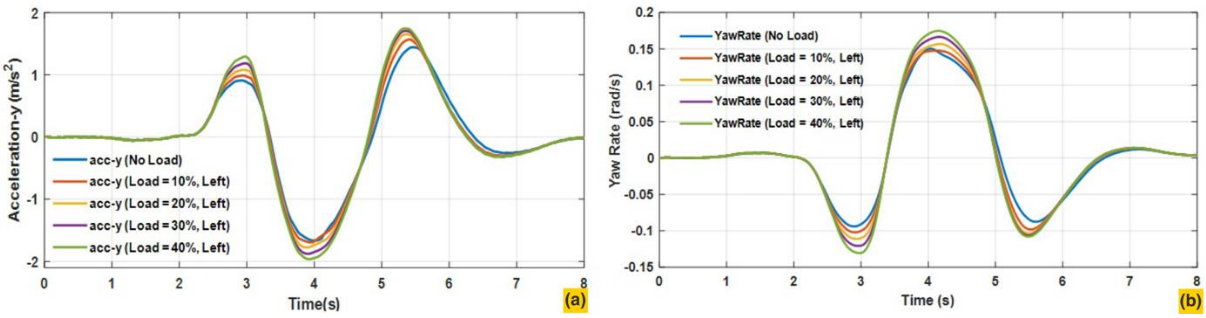

Figure 25. Effect of additional load disturbance at the left wheel of the vehicle for $V = 50$ km/h: (a) Lateral acceleration of the vehicle and (b) Yaw rate of the vehicle

4 illustrate the impact of the initial load and increasing additional load transfer to the opposite side of the vehicle's trajectory and lateral acceleration. Phase 1 shows that the lateral acceleration of the no-load condition is lower than that of other conditions, as higher load percentages are initially applied at either side of the wheel until the vehicle reaches 2.6 s. At this point, the driver countersteers to turn the vehicle in the right direction to exit the lane. The harsh countersteer from the driver causes the load to transfer from the right side to the left side of the vehicle. Phase 2 displays the vehicle's yaw rate and lateral acceleration. There is a slight

difference between the no-load condition and the additional load condition until the vehicle reaches 3.5 s, at which the driver countersteers to change the vehicle direction from right to left to enter the lane. The harsh countersteer produces a significant weight transfer to the opposite side of the vehicle's direction. Phase 3 illustrates that once the vehicle steers to the left, the effect from the previous phase still influences lateral acceleration and yaw rate. Due to the aggressive steer from the driver in Phase 3, there is a significant load transfer effect from the left to the right until the vehicle reaches 4.8 s, when the driver initiates a countersteer to the right. This significantly affects the yaw rate and lateral acceleration, causing the additional load condition to deviate from the values observed during the no-load condition. Phase 5 visualises the effects of yaw rate and lateral acceleration when the driver slightly countersteers to the right. In contrast to **Figure 9b**, which depicts the pattern of the steer wheel input data from the driver while the vehicle drives at approximately 30 km/h, **Figure 11b** displays unaggressive steer, specifically for a velocity of 50 km/h. However, at a certain time range, the harsh steer from the driver, as mentioned above, indicates a significant difference in lateral acceleration and yaw rate between the additional load condition and the no-load condition.

The trajectory of the vehicle travelling at 50 km/h is shown in **Figure 26**. When avoiding an obstacle, the vehicle's reference trajectory, devoid of any additional weight transfer phenomena, is represented by the black dotted line. The yellow rectangle with a red dotted line represents the obstacle. The turquoise and blue dotted lines illustrate the vehicle's trajectory when a 10% additional load is added at the right and left sides of the wheels, respectively. The orange and chocolate dotted lines indicate the vehicle's trajectory with a 20% additional load at the right and left sides of the wheels, respectively. The green and dark green dotted lines represent the vehicle's trajectory when a 30% additional load is added at the right and left sides of the wheels, respectively. The pink and red dotted lines represent the vehicle's trajectory when a 40% additional load is added at the right and left sides of the wheels, respectively. All trajectories at all load percentages experience understeer while avoiding the obstacle and successfully preventing a collision with the road barrier during the CA scenario.

6. Conclusion

This paper examines the effect of additional load distribution disturbances on vehicle trajectory while avoiding an obstacle. A CA scenario was simulated in MATLAB Simulink, corresponding to real-time experiments. A nonlinear vehicle model was developed in the simulation by incorporating Dugoff's nonlinear tyre characteristics and a load transfer model to enhance reliability and reduce the uncertainty of the model during the CA scenario. The results emphasise that additional load disturbances at each tyre can reduce vehicle stability while navigating. The combination of additional lateral forces caused by extra load placement and load transfer phenomena can amplify oversteer or understeer when avoiding obstacles. These findings show that implementing a proper control strategy to the system can prevent the vehicle from disaster, especially in extreme manoeuvring

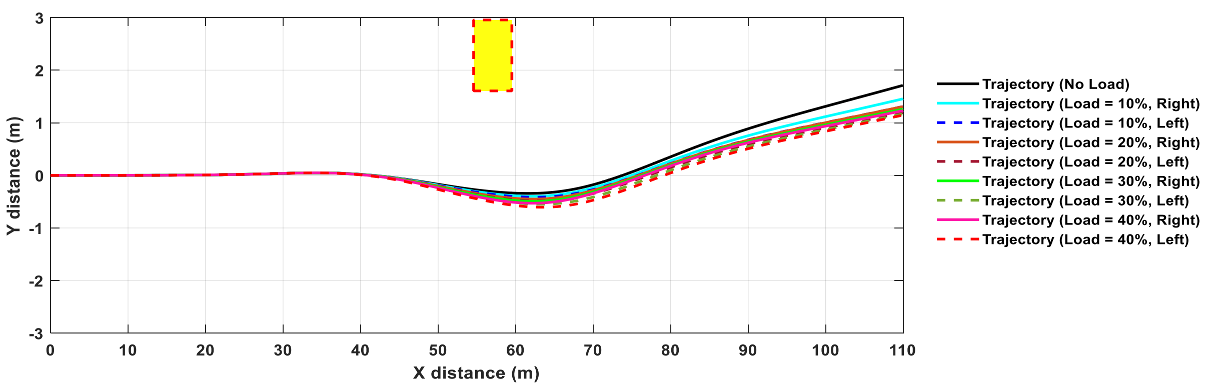

Figure 26. Vehicle's trajectories with additional load at 50 km/h

scenarios. This study lays the foundation for future studies focusing on designing robust disturbance rejection controllers to reject disturbance corresponding to vehicle dynamics characteristics, thereby enhancing the safety and smoothness of vehicle navigation while avoiding obstacles.

Acknowledgements

The authors would like to thank the Ministry of Higher Education Malaysia for providing the Fundamental Research Grant Scheme (FRGS/1/2022/TK10/UMP/02/27) (RDU220116). Special thanks are also extended to the Autonomous Laboratory, Universiti Malaysia Pahang Al-Sultan Abdullah for providing the facilities to conduct this study.

Author's Declaration

Authors' contributions and responsibilities

The authors made substantial contributions to the conception and design of the study. The authors took responsibility for data analysis, interpretation and discussion of results. The authors read and approved the final manuscript.

Funding

Ministry of Higher Education Malaysia with Fundamental Research Grant Scheme (FRGS/1/2022/TK10/UMP/02/27) (RDU220116).

Availability of data and materials

All data are available from the authors.

Competing interests

The authors declare no competing interest.

Additional information

No additional information from the authors.

References

[1] N. Che-Him *et al.*, "Factors Affecting Road Traffic Accident in Batu Pahat, Johor, Malaysia," *Journal of Physics: Conference Series*, vol. 995, p. 012033, Apr. 2018, doi: 10.1088/1742-6596/995/1/012033.

[2] E. Yong *et al.*, "Investigation of the Vehicle Driving Trajectory During Turning at Intersectional Roads Using Deep Learning Model," *Automotive Experiences*, vol. 7, no. 1, pp. 63–76, Apr. 2024, doi: 10.31603/ae.10649.

[3] N. Md Yusof *et al.*, "Effect of Road Darkness on Young Driver Behaviour when Approaching Parked or Slow-moving Vehicles in Malaysia," *Automotive Experiences*, vol. 6, no. 2, pp. 216–233, May 2023, doi: 10.31603/ae.8206.

[4] F. H. K. Kamaru Zaman *et al.*, "Malaysian Public's Perception Toward Event Data Recorder (EDR) in Vehicles," *Automotive Experiences*, vol. 7, no. 3, pp. 513–524, Dec. 2024, doi: 10.31603/ae.11706.

[5] S. I. Mohammed, "An Overview of Traffic Accident Investigation Using Different Techniques," *Automotive Experiences*, vol. 6, no. 1, pp. 68–79, Jan. 2023, doi: 10.31603/ae.7913.

[6] M. Mutharuddin *et al.*, "The Road Safety: Utilising Machine Learning Approach for Predicting Fatality in Toll Road Accidents," *Automotive Experiences*, vol. 7, no. 2, pp. 236–251, 2024, doi: 10.31603/ae.11082.

[7] M. C. Jia Ying, W. Kean Yew, P. J. Yew, and A. Yang Her, "Real-time road accident reporting system with location detection using cloud-based data analytics," in *IECON 2022 – 48th Annual Conference of the IEEE Industrial Electronics Society*, IEEE, Oct. 2022, pp. 1–6. doi: 10.1109/IECON49645.2022.9968507.

[8] N. Ikhsan, A. S. Abdullah, and R. Ramli, "The effect of gross vehicle weight on the stability of heavy vehicle during cornering," *International Journal of Mechanical and Mechatronics Engineering*, vol. 9, no. 7, pp. 1251–1256, 2015.

[9] M. G. Masuri, A. Dahlan, A. Danis, and K. A. M. Isa, "Public Participation in Shaping Better Road Users in Malaysia," *Procedia - Social and Behavioral Sciences*, vol. 168, pp. 341–348, Jan. 2015, doi: 10.1016/j.sbspro.2014.10.239.

[10] N. Lin, C. Zong, M. Tomizuka, P. Song, Z. Zhang, and G. Li, "An Overview on Study of Identification of Driver Behavior Characteristics for Automotive Control," *Mathematical Problems in Engineering*, vol. 2014, no. 1, pp. 1–15, Jan. 2014, doi: 10.1155/2014/569109.

[11] S. S. Lodhi, N. Kumar, and P. K. Pandey, "Autonomous vehicular overtaking maneuver: A survey and taxonomy," *Vehicular Communications*, vol. 42, p. 100623, Aug. 2023, doi:

10.1016/j.vehcom.2023.100623.

[12] U. Z. Abdul Hamid, K. Pushkin, H. Hamzuri, D. Gueraiche, and M. A. Abdul Rahman, "Current Collision Mitigation Technologies for Advanced Driver Assistance Systems – A Survey," *PERINTIS eJournal*, vol. 6, no. 2, pp. 78–90, 2016.

[13] C. Wang, J. Delport, and Y. Wang, "Lateral Motion Prediction of On-Road Preceding Vehicles: A Data-Driven Approach," *Sensors*, vol. 19, no. 9, p. 2111, May 2019, doi: 10.3390/s19092111.

[14] J. A. Michon, "A critical view of driver behavior models: what do we know, what should we do?," in *Human Behavior and Traffic Safety*, New York: Springer, 1985, pp. 485–524.

[15] K. Rumar, "The role of perceptual and cognitive filters in observed behavior," in *Human Behavior and Traffic Safety*, H. behavior and traffic safety, Ed., North-Holland, 1985, pp. 151–170.

[16] M. Hosseinpour, A. S. Yahaya, A. F. Sadullah, N. Ismail, and S. M. R. Ghadiri, "Evaluating the effects of road geometry, environment, and traffic volume on rollover crashes," *Transport*, vol. 31, no. 2, pp. 221–232, Jun. 2016, doi: 10.3846/16484142.2016.1193046.

[17] U. Z. Abdul Hamid, H. Hamzuri, M. A. A. Rahman, and W. J. Yahya, "A safe-distance based threat assessment with geometrical based steering control for vehicle collision avoidance," *Journal of Telecommunication, Electronic and Computer Engineering (JTEC)*, vol. 8, no. 2, pp. 53–58, 2016.

[18] U. Z. A. Hamid, Y. Saito, H. Zamzuri, M. A. A. Rahman, and P. Raksincharoensak, "A review on threat assessment, path planning and path tracking strategies for collision avoidance systems of autonomous vehicles," *International Journal of Vehicle Autonomous Systems*, vol. 14, no. 2, p. 134, 2018, doi: 10.1504/IJVAS.2018.096154.

[19] U. Z. Abdul Hamid, H. Zamzuri, T. Yamada, M. A. Abdul Rahman, Y. Saito, and P. Raksincharoensak, "Modular design of artificial potential field and nonlinear model predictive control for a vehicle collision avoidance system with move blocking strategy," *Proceedings of the Institution of Mechanical Engineers, Part D: Journal of Automobile Engineering*, vol. 232, no. 10, pp. 1353–1373, Sep. 2018, doi: 10.1177/0954407017729057.

[20] K. Zheng, B. Zhou, X. Wu, T. Chai, and Q. Pan, "A humanoid collision-avoidance strategy considering a large sideslip angle state," *Control Engineering Practice*, vol. 138, p. 105623, Sep. 2023, doi: 10.1016/j.conengprac.2023.105623.

[21] A. Zulkifli, M. H. Peeie, M. A. Zakaria, M. I. Ishak, M.A. Shahrom, and B. Kujunni, "Motion Planning and Tracking Trajectory of an Autonomous Emergency Braking Pedestrian (AEB-P) System Based on Different Brake Pad Friction Coefficients on Dry Road Surface," *International Journal of Automotive and Mechanical Engineering*, vol. 19, no. 3, Oct. 2022, doi: 10.15282/ijame.19.3.2022.12.0772.

[22] Y. Saito and P. Raksincharoensak, "Shared Control in Risk Predictive Braking Maneuver for Preventing Collisions With Pedestrians," *IEEE Transactions on Intelligent Vehicles*, vol. 1, no. 4, pp. 314–324, Dec. 2016, doi: 10.1109/TIV.2017.2700210.

[23] U. Z. Abdul Hamid, Y. Saito, and P. Raksina Charoensak, "Collision avoidance performance analysis of a varied loads autonomous vehicle using integrated nonlinear controller," *PERINTIS eJournal*, vol. 8, no. 1, pp. 25–43, 2018.

[24] B. Kunjunni, M. A. bin Zakaria, A. P. . Majeed, A. F. A. Nasir, M. H. Bin Peeie, and U. Z. Abdul Hamid, "Effect of load distribution on longitudinal and lateral forces acting on each wheel of a compact electric vehicle," *SN Applied Sciences*, vol. 2, no. 2, p. 244, Feb. 2020, doi: 10.1007/s42452-020-1996-9.

[25] J. Wang, Z. Luo, Y. Wang, B. Yang, and F. Assadian, "Coordination Control of Differential Drive Assist Steering and Vehicle Stability Control for Four-Wheel-Independent-Drive EV," *IEEE Transactions on Vehicular Technology*, vol. 67, no. 12, pp. 11453–11467, Dec. 2018, doi: 10.1109/TVT.2018.2872857.

[26] J. Samsundar and J. C. Huston, "Estimating Lateral Stability Region of a Nonlinear 2

Degree-of-Freedom Vehicle," *SAE Transactions*, vol. 107, pp. 1791–1797, Apr. 1998.

[27] Z. Sun, J. Zou, D. He, Z. Man, and J. Zheng, "Collision-avoidance steering control for autonomous vehicles using neural network-based adaptive integral terminal sliding mode," *Journal of Intelligent & Fuzzy Systems*, vol. 39, no. 3, pp. 4689–4702, Oct. 2020, doi: 10.3233/JIFS-200625.

[28] X. Wu, B. Zhou, G. Wen, L. Long, and Q. Cui, "Intervention criterion and control research for active front steering with consideration of road adhesion," *Vehicle System Dynamics*, vol. 56, no. 4, pp. 553–578, Apr. 2018, doi: 10.1080/00423114.2017.1395465.

[29] R. Rajamani, *Vehicle Dynamics and Control*, 2nd ed., vol. 2nd Edition. in Mechanical Engineering Series, vol. 2nd Edition. Boston, MA: Springer US, 2012. doi: 10.1007/978-1-4614-1433-9.

[30] I. M. Zulhilmi, P. M. Heerwan, S. M. Asyraf, I. M. Sollehudin, and I. M. Ishak, "Experimental study on the effect of emergency braking without anti-lock braking system to vehicle dynamics behaviour," *International Journal of Automotive and Mechanical Engineering*, vol. 17, no. 2, pp. 7832–7841, Apr. 2020, doi: https://doi.org/10.15282/ijame.17.2.2020.02.0583.